J. Fluid Mech. (1984), *vol.* 143, *pp.* 125–152
Printed in Great Britain

Roll-pattern evolution in finite-amplitude Rayleigh–Beńard convection in a two-dimensional fluid layer bounded by distant sidewalls

By P. G. DANIELS

Department of Mathematics, The City University, Northampton Square, London EC1V 0HB

(Received 16 October 1982 and in revised form 1 August 1983)

This paper considers the temporal evolution of two-dimensional Rayleigh–Bénard convection in a shallow fluid layer of aspect ratio $2L$ ($\gg 1$) confined laterally by rigid sidewalls. Recent studies by Cross *et al.* (1980, 1983) have shown that for Rayleigh numbers in the range $R = R_0 + O(L^{-1})$ (where R_0 is the critical Rayleigh number for the corresponding infinite layer) there exists a class of finite-amplitude steady-state 'phase-winding' solutions which correspond physically to the possibility of an adjustment in the number of rolls in the container as the local value of the Rayleigh number is varied. It has been shown (Daniels 1981) that in the temporal evolution of the system the final lateral positioning of the rolls occurs on the long timescale $t = O(L^2)$ when the phase function which determines the number of rolls in the system satisfies a one-dimensional diffusion equation but with novel boundary conditions that represent the effect of the sidewalls. In the present paper this system is solved numerically in order to determine the precise way in which the roll pattern adjusts after a change in the Rayleigh number of the system. There is an interesting balance between, on the one hand, a tendency for the number of rolls to change by the least number possible and, on the other, a tendency for the even or odd nature of the initial configuration to be preserved during the transition. In some cases this second property renders the natural evolution susceptible to arbitrarily small external disturbances, which then dictate the form of the final roll pattern.

The complete transition involves an analysis of the motion on three timescales, a conductive scale $t = O(1)$, a convective growth scale $t = O(L)$ and a convective diffusion scale $t = O(L^2)$.

1. Introduction

Although the subject of hydrodynamic stability and the transition from laminar to turbulent flow continues to attract considerable theoretical and experimental attention, there is still an incomplete understanding of the mechanics of roll-pattern adjustment in slightly supercritical flows between, for example, rotating cylinders or heated planes. The intriguing series of flow patterns with different numbers of Taylor vortices and wavy vortices observed by Coles (1965) in his experiments on the flow between rotating cylinders has never been satisfactorily explained and in the Rayleigh–Bénard problem, similar transitions in the concentric roll pattern in a shallow cylinder observed by Koschmieder & Pallas (1974) still offer a challenge to the theoretician. There has been much recent work on roll-pattern formation in the Rayleigh–Bénard problem, but although numerical simulations (Normand 1981; Siggia & Zippelius 1981; Greenside, Coughran & Schryer 1982) and semidescriptive

arguments (Cross 1982) can provide a valuable insight into the rich variety of possible flow configurations, a theoretical description based on a formal asymptotic solution of the Navier–Stokes equations is clearly desirable. Unfortunately, theoretical progress is made difficult by the complexities of even the simplest realistic models, since nonlinear effects, geometrical constraints and the multiplicity of solutions are all essential ingredients of this type of flow.

In the Rayleigh–Bénard problem in which convection is induced in a horizontal fluid layer by uniform heating from below, it has been established in recent years (Daniels 1977, 1978, 1981; Brown & Stewartson 1977; Cross *et al.* 1980, 1983; Cross 1982) that, even in containers of large horizontal dimensions, the lateral walls can have a significant influence on the flow pattern that develops when the Rayleigh number R exceeds its critical value. Thus results for the corresponding infinite layer cannot, in general, be used to make predictions about either the detailed structure or the stability of the roll pattern in practical situations. A major advance in the theoretical understanding of convective flows in finite geometries was made when Segel (1969) demonstrated how distant lateral walls could be incorporated in a description of the finite-amplitude motion at slightly supercritical Rayleigh numbers based on the use of multiple scaling techniques. A similar formulation was adopted in a related study by Newell & Whitehead (1969). In the present work attention is restricted to the case of two-dimensional motion in the form of rolls parallel to rigid, perfectly insulated lateral walls; Segel's results provide a description of the motion in the range $R-R_0 = O(L^{-2})$, where L is the (large) semi-aspect ratio of the container and R_0 is the critical Rayleigh number for the corresponding infinite layer. At the lateral walls it is found that the amplitude function A defining the strength of the convective motion across the layer must vanish. The main properties of the steady solution are, first, an $O(L^{-2})$ increase in the critical Rayleigh number over that for the infinite layer due to the presence of the lateral walls, and, secondly, an amplitude profile which adjusts from an infinitesimal sinusoidal form at the onset of motion to the familiar finite-amplitude form of magnitude $(R-R_0)^{\frac{1}{2}}$ as $(R-R_0)L^2 \to \infty$; at this point the profile A is virtually uniform across the container, the adjustment to the lateral boundary conditions being made in the vicinity of the sidewalls.

In order to obtain a precise description of the number of rolls in the system it is actually necessary to consider higher-order terms in the solution and match these to appropriate boundary-layer solutions valid near each sidewall (Daniels 1978). It is found that four solutions evolve from the neighbourhood of the Rayleigh number $R_1 = R_0 + O(L^{-2})$, two of which correspond to an even number of rolls and two to an odd number of rolls. These solutions bifurcate at $R = R_1 \pm O(L^{-3})$, but only the pair that stem from the lower, critical value of R are stable to two-dimensional disturbances (this pair may be even or odd depending on the precise value of L). In the range $R-R_0 = O(L^{-2})$ other steady convective solutions become possible and may be expressed in terms of Jacobian elliptic functions (Segel 1969), but it appears that these are all unstable (Daniels 1977), such solutions having positions of zero amplitude in the interior of the container.

Knowledge of the higher-order terms mentioned above also provides a means of determining the range of validity of the asymptotic expansions which form the basis of the solution for $R-R_0 = O(L^{-2})$. It emerges (Cross *et al.* 1980, 1983; Daniels 1981, appendix) that when $R-R_0 = O(L^{-1})$ a new regime evolves in which the motion near the sidewalls is sufficiently strong to provoke a reaction that requires an adjustment in the roll pattern throughout the container. In preparation for the more detailed analysis to be presented below, it is perhaps useful at this stage to understand how

the different regimes arise in the context of the familiar amplitude equation governing slightly supercritical flows. For two-dimensional motion with stress-free horizontal boundaries, and with

$$R-R_0 = 18\pi^2\delta L^{-2}, \quad x = LX, \quad t = \frac{1+P}{4P}L^2\tau, \tag{1.1}$$

where x and t are appropriate non-dimensional length- and timescales and P is the Prandtl number, this equation has the form

$$A_\tau = A_{XX} + \delta A - A|A|^2. \tag{1.2}$$

Use of the polar form $A(X,\tau) = \rho e^{i\phi}$ then gives

$$\rho_\tau = \rho_{XX} - \rho\phi_X^2 + \delta\rho - \rho^3, \tag{1.3}$$

$$\rho\phi_\tau = \rho\phi_{XX} + 2\rho_X\phi_X, \tag{1.4}$$

and since the solution for the non-dimensional stream function ψ has the form

$$\psi = 4i\pi^{-1}L^{-1}\rho\exp\left\{\frac{i\pi x}{\sqrt{2}} + i\phi\right\}\sin\pi z + \text{c.c.}, \tag{1.5}$$

it can be seen that ρ effectively represents the strength of the convection and ϕ determines any adjustment in wavelength. In the regime considered by Segel (1969) and Daniels (1978) where $\delta = O(1)$, all of the terms in (1.3) and (1.4) are of equal importance and solutions must satisfy $\rho(\pm 1,\tau) = 0$. In the steady state this leads to the requirement that ϕ is constant in (1.3) and (1.4), and so the wavelength of convection remains at the critical value of $\sqrt{2}$.

As δ increases, the steady-state solution of (1.3) is dominated by the last two terms, so that $\rho \sim \delta^{\frac{1}{2}}$ except in boundary layers near the lateral walls. Furthermore, this steady state is likely to be achieved on the relatively short timescale of $\tau \sim \delta^{-1}$. Thereafter, since $\rho_X \approx 0$, (1.4) is dominated by the first two terms and, on the longer timescale $\tau \sim 1$, can lead to a steady-state solution in which ϕ is a linear function of X:

$$\phi = qX + C. \tag{1.6}$$

The value of q is associated with the number of rolls in the container since the effective wavelength in (1.5) is $\sqrt{2} - 2\pi^{-1}qL^{-1}$ and thus there are, roughly speaking,

$$\sqrt{2}\,L + 2\pi^{-1}q \tag{1.7}$$

rolls contained between the lateral walls $x = \pm L$. In order to determine q it is necessary to calculate the flow induced near the lateral walls by the core solution $\rho \sim \delta^{\frac{1}{2}}$. For $\delta \ll L$ the reaction is essentially passive, leads to a zero value of q in (1.6), and thus (as stated above) no change in the wavelength of the roll pattern from the critical value $\sqrt{2}$. However, for $\delta = O(L)$ the sidewall interaction is found to be sufficient to generate non-zero values of q and solutions with different numbers of rolls, (1.7), become possible. These steady-state solutions were first established by Cross *et al.* (1980) and designated 'phase-winding' solutions in view of the horizontal variation involved in (1.6). Full details of the formal asymptotic structure including the sidewall interaction which involves consideration of double boundary-layer regions near each lateral wall, are given in a later paper (Cross *et al.* 1983).

In the range $R - R_0 = O(L^{-1})$, then, it is found that the four solutions stemming from the neighbourhood of R_1 are joined by a whole new family of solutions, all with the same (uniform) strength across the width of the container, but containing

different numbers of rolls. Stability considerations can be used to rule out the physical occurrence of a certain proportion of these phase-winding solutions (Daniels 1981), but in general, at a given value of the Rayleigh number in the range $R-R_0 = O(L^{-1})$, there remains a multiple choice of steady-state solutions which are stable to two-dimensional disturbances. Thus the selection of a particular steady state can only be guaranteed by an analysis of the evolutionary properties of the system; it is this analysis which is undertaken in the present investigation. One of the more interesting findings is that after a change in the Rayleigh number there is not a direct preference for the number of rolls to change by the minimum number possible, consistent with the attainment of a stable steady state. Instead the preservation of the even or odd nature of the initial configuration is found to be of primary significance, with a possible transition from an even to an odd solution (or vice versa) only if dictated by the requirements of stability.

The governing equations and boundary conditions are stated in §2. It is assumed that initially the Rayleigh number lies in the range $R-R_0 = O(L^{-1})$ so that one of the steady-state phase-winding solutions is established in the container. This initial state is also described in §2. At time $t = 0$ the temperature of the lower surface is raised by an amount $O(L^{-1})$, causing an effective increase in the Rayleigh number of the same magnitude. The subsequent evolution of the system is then shown to occur on three timescales. The first, when $t = O(1)$, corresponds to the conductive timescale needed to establish the new basic temperature profile in the container and is described in §3. This change then initiates the second stage of evolution on the longer timescale $t = O(L)$, when the strength of the convective motion is adjusted to a size appropriate to the new value of the Rayleigh number throughout the container. This is described in §4. In the main body of the fluid (or core) this change has no effect on the roll pattern established at $t = 0$, although an analysis of the motion in the boundary layers near each sidewall (§5) demonstrates that an interaction is initiated there that begins to influence the roll pattern. The influence gradually penetrates from each sidewall inwards into the core until, on the timescale $t = O(L^2)$, a new roll pattern evolves there. Although this final evolution, described in §6, is governed by a linear diffusion equation for the 'phase function' ϕ, it is rendered nonlinear by the form of the boundary conditions that result from matching with solutions in the boundary layers near each sidewall. Some of the basic properties of this final evolutionary system are discussed in §7, and these assist in the interpretation of full numerical solutions of the system, described in §8. Analytic solutions are possible in certain limiting cases and these are outlined in Appendices A and B. The results are discussed in §9.

2. Governing equations and initial state

The motion that evolves in the region $0 \leqslant z \leqslant 1$, $-L \leqslant x \leqslant L$ is governed by the two-dimensional Oberbeck–Boussinesq equations:

$$\left.\begin{aligned} u_x + w_z &= 0, \\ u_t + uu_x + wu_z &= -p_x + P\nabla^2 u, \\ w_t + uw_x + ww_z &= -p_z + P\nabla^2 w + PT, \\ T_t + uT_x + wT_z - Rw &= \nabla^2 T, \end{aligned}\right\} \tag{2.1}$$

where the Cartesian coordinates (x, z), time t, velocity components (u, w), reduced pressure p and perturbation T from the linear conductive temperature profile are

non-dimensionalized with respect to the quantities d, d^2/κ, κ/d, $\tilde{\rho}\kappa^2/d^2$ and $\kappa\nu/\tilde{\alpha}gd^3$ respectively, where d is the height of the container, κ is the thermal diffusivity of the fluid, ν is the kinematic viscosity, $\tilde{\rho}$ is the density, $\tilde{\alpha}$ is the coefficient of thermal expansion and g is the acceleration due to gravity. The Rayleigh number R and Prandtl number P are defined by

$$R = \frac{\tilde{\alpha}gd^3(T_1 - T_0)}{\nu\kappa}, \quad P = \frac{\nu}{\kappa}, \tag{2.2}$$

where $T_0 < T_1$ are the constant temperatures of the upper and lower surfaces. These are assumed stress-free so that

$$w = u_z = T = 0 \quad (z = 0, 1). \tag{2.3}$$

The sidewalls are taken to be rigid and perfectly insulating:

$$u = w = T_x = 0 \quad (x = \pm L). \tag{2.4}$$

A stream function ψ is defined by

$$u = \psi_z, \quad w = -\psi_x, \quad \psi = 0 \quad \text{at} \quad (0, 0). \tag{2.5}$$

The non-dimensional temperature field measured from zero at the lower surface is

$$\theta = -Rz + T. \tag{2.6}$$

We shall be concerned with solutions for Rayleigh numbers in the range

$$R = R_0 + 18\pi^2 \Delta L^{-1}, \quad \Delta = O(1), \tag{2.7}$$

where $R_0 = \frac{27}{4}\pi^4$ is the critical Rayleigh number for the corresponding infinite layer, and $L \gg 1$. Let us assume that initially one of the steady-state solutions described by Cross *et al.* (1983) is established in the container at a finite value of Δ:

$$\Delta = \Delta_0. \tag{2.8}$$

It should be noted that the expansions given by Cross *et al.* (1983) are based on the small parameter $\epsilon = \Delta L^{-1}$ and the large parameter L, but here it is more convenient to use the single large parameter L and allow the variable parameter Δ to represent changes in the Rayleigh number in the range under consideration. The results of Cross *et al.* (1983) are then easily adapted to give the asymptotic structure of the initial flow pattern as follows.

In the main body of the fluid (or core), where

$$X = L^{-1}x = O(1), \tag{2.9}$$

the stream function is given by

$$\psi = L^{-\frac{1}{2}} 4i\pi^{-1}(A_0 e^{i\pi x/\sqrt{2}} - A_0^* e^{-i\pi x/\sqrt{2}}) \sin \pi z + O(L^{-1}), \tag{2.10}$$

where $*$ denotes complex conjugate and

$$A_0 = \Delta_0^{\frac{1}{2}} e^{i\phi_0(X)}, \quad \phi_0 = q_0 X + C_0. \tag{2.11}$$

At $X = -1$ this solution matches with that in a boundary-layer region where

$$\tilde{X} = L^{\frac{1}{2}}(x + L) = O(1) \tag{2.12}$$

and

$$\psi = L^{-\frac{1}{2}} 4i\pi^{-1}\{(\tilde{A}_0 + L^{-\frac{1}{2}}\tilde{A}_1) e^{i\pi x/\sqrt{2}} - (\tilde{A}_0^* + L^{-\frac{1}{2}}\tilde{A}_1^*) e^{-i\pi x/\sqrt{2}}\} \sin \pi z + O(L^{-\frac{3}{2}}), \tag{2.13}$$

where

$$\tilde{A}_0 = \Delta_0^{\frac{1}{2}} e^{i\phi_0(-1)} \tanh \frac{\Delta_0^{\frac{1}{2}} \tilde{X}}{\sqrt{2}} \tag{2.14}$$

and

$$\tilde{A}_1 = \Delta_0 e^{i\phi_0(-1)} \{\tilde{\alpha}_r(\Delta_0^{\frac{1}{2}} \tilde{X}) + i\tilde{\alpha}_i(\Delta_0^{\frac{1}{2}} \tilde{X})\}. \tag{2.15}$$

Here

$$\tilde{\alpha}_r(\tilde{X}) = \tilde{a} \operatorname{sech}^2 \frac{\tilde{X}}{\sqrt{2}}, \tag{2.16}$$

$$\tilde{\alpha}_i(\tilde{X}) = \tilde{b}\left(\tilde{X} \tanh \frac{\tilde{X}}{\sqrt{2}} - \sqrt{2}\right) + \tilde{c} \tanh \frac{\tilde{X}}{\sqrt{2}} + I(\tilde{X}), \tag{2.17}$$

where $\tilde{a}$, $\tilde{b}$ and $\tilde{c}$ are real constants,

$$I(\tilde{X}) = K_1 + K_2\left(\tanh \frac{\tilde{X}}{\sqrt{2}} + \tfrac{1}{2} \operatorname{sech}^2 \frac{\tilde{X}}{\sqrt{2}}\right), \tag{2.18}$$

and

$$K_1 = \frac{1}{\sqrt{2}}(k_1 + 2k_2 - 2k_3 - k_4 - k_5), \quad K_2 = \frac{1}{\sqrt{2}}(-3k_2 + 2k_3 + k_4 + k_5), \tag{2.19}$$

where

$$k_1 = \frac{2\sqrt{2}}{\pi}, \quad k_2 = \frac{22}{9\sqrt{2}\,\pi}, \quad k_3 = \frac{(\frac{9}{8} + P^{-1})(15P^{-1} - 9)}{36\sqrt{2}\,\pi}, \quad k_4 = 5k_5 = \frac{25}{3\sqrt{2}\,\pi}. \tag{2.20}$$

At $\tilde{X} = 0$ this boundary-layer solution matches with that in a sidewall region where $x_1 = x + L = O(1)$ and

$$\psi = L^{-1}\psi_0 + \ldots, \tag{2.21}$$

$$\psi_0 = 4i\pi^{-1}\Delta_0\{(ax_1 + b) e^{i\pi x/\sqrt{2}} - (a^* x_1 + b^*) e^{-i\pi x/\sqrt{2}} + id\, e^{-2\pi x_1}\} \sin \pi z, \tag{2.22}$$

and where matching with (2.13) requires that

$$\Delta_0 a = \tilde{A}_{0\tilde{X}}(\tilde{X} = 0), \quad \Delta_0 b = \tilde{A}_1(\tilde{X} = 0). \tag{2.23}$$

The three boundary conditions (2.4) at $x_1 = 0$ also lead to the relation

$$b = -\alpha^* a - \beta^* a^*, \tag{2.24}$$

where

$$\alpha = \alpha_r + i\alpha_i = (-16 + 5\sqrt{2}\, i)/18\pi \tag{2.25}$$

and

$$\beta = \beta_r + i\beta_i = |\beta| e^{i\chi} = -(16 + 13\sqrt{2}\, i) e^{-i\pi\sqrt{2}L}/18\pi. \tag{2.26}$$

The real constant d can be expressed in terms of b as

$$d = ib\, e^{-i\pi L/\sqrt{2}} - ib^* e^{i\pi L/\sqrt{2}}. \tag{2.27}$$

The whole system is closed by completing the matching between $\tilde{A}_1$ and the core solution (2.10) and carrying out a similar analysis of the boundary-layer and sidewall regions near $x = L$. In the boundary-layer solution (2.13) the constants $\tilde{a}$ and $\tilde{b}$ are determined as

$$\left.\begin{aligned} \tilde{a} &= -\frac{1}{\sqrt{2}}(\alpha_r + |\beta| \cos\{2\phi_0(-1) + \chi\}), \\ \tilde{b} &= -\tfrac{1}{2}(\alpha_0 + |\beta| \sin\{2\phi_0(-1) + \chi\}), \end{aligned}\right\} \tag{2.28}$$

where

$$\alpha_0 = \alpha_i - \sqrt{2}\, I(0) = (5 + 21P^{-1} + 40P^{-2})/96\sqrt{2}\,\pi, \tag{2.29}$$

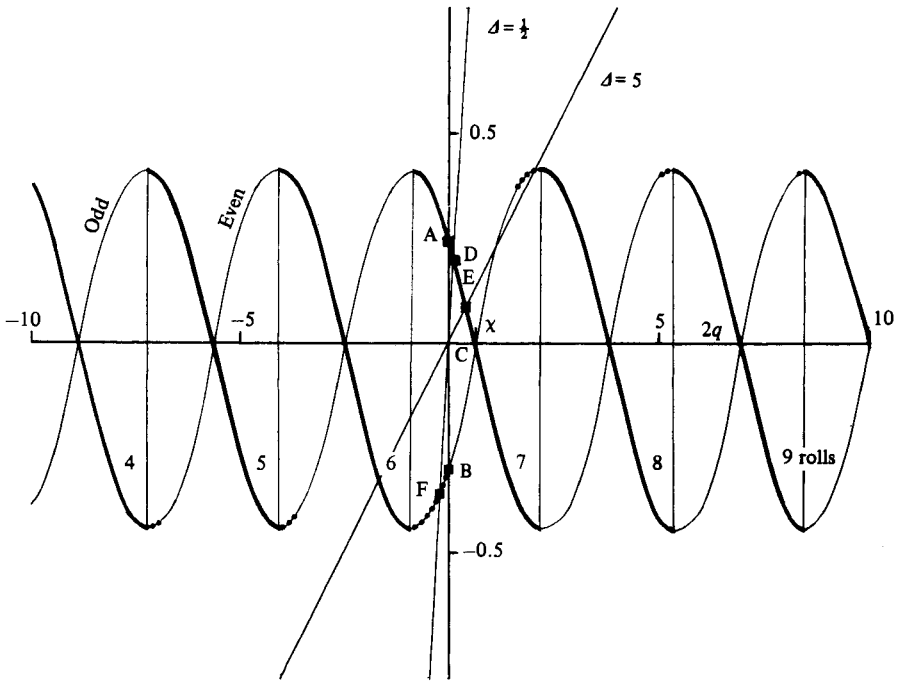

FIGURE 1. Steady-state solutions for a case corresponding to $L = 5$ and $P = 10$. Solutions at a given value of Δ are given by the points of intersection of the appropriate sloping line of gradient Δ^{-1} (those for $\Delta = 0.5$ and $\Delta = 5$ are shown) with the sinusoidal curves (class I solutions) or the vertical lines (class II solutions). The light sections are unstable to odd or even disturbances in ϕ, while the dotted sections are only unstable to even disturbances in ϕ (see §7). The heavy sections are stable and correspond to flows with the given number of rolls. There are two solutions at each point of intersection with a sinusoidal curve and four at each intersection with a vertical line.

although $\tilde{c}$ remains undetermined at this stage of the expansion. In the core solution (2.11) two sets of values of q_0 and C_0 are found to be possible.

In the first set (class I solution)

$$2q_0 = -\Delta_0(\alpha_0 - (-1)^n|\beta|\sin\{2q_0 - \chi\}), \quad C_0 = \tfrac{1}{2}n\pi \quad (n = 0, 1, 2, 3). \tag{2.30}$$

Here only four values of n represent distinct solutions since an increase in C_0 by 2π has no effect on (2.10). The $n = 0$ and $n = 2$ solutions are equal and opposite flows with an even number of rolls, the vertical component of velocity being symmetric about $x = 0$ to leading order, from (2.10). The $n = 1$ and $n = 3$ solutions are equal and opposite flows, but with an odd number of rolls. These solutions will be referred to as even and odd solutions respectively.

In the second set (class II solution)

$$2q_0 = \chi - \tfrac{1}{2}\pi + m\pi = -\Delta_0(\alpha_0 - (-1)^m|\beta|\cos 2C_0) \tag{2.31}$$

Here a discrete set of solutions exists for integer values of m, each having a constant value of q_0. The corresponding range of values of Δ_0 is restricted by the inequality $|2q_0\Delta_0^{-1} + \alpha_0| < |\beta|$ and is traversed as the value of C_0 varies by $\frac{1}{2}\pi$. These solutions, which are neither even nor odd, therefore connect the even and odd class I solutions, as may be seen from a graphical construction of the steady-state solutions (2.30) and (2.31) for two typical cases in figures 1 and 2. A solution (2.30) or (2.31) corresponds

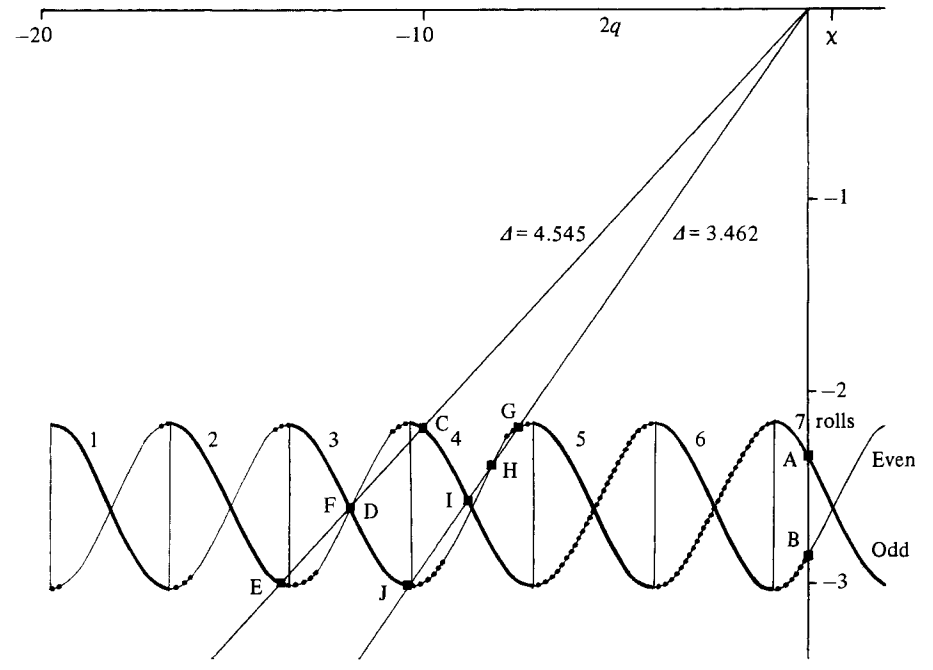

FIGURE 2. Steady-state solutions for a case corresponding to $L = 5$ and $P = 0.2$.

to a point of intersection of a straight line of gradient $\Delta^{-1} = \Delta_0^{-1}$ with one of the sinusoidal curves representing the right-hand side of (2.30) or vertical lines representing the right-hand side of (2.31). Figures 1 and 2 will be discussed in greater detail in §§7, 8 but it is worth noting the crucial nature of the value of the Prandtl number which, through the value of α_0 in (2.29), determines whether an evolution with a constant number of rolls is possible (figure 1) or whether the number of rolls must change as the Rayleigh number is increased (figure 2).

3. Evolution of the base state: $t = O(1)$

A steady state of the type described in §2, equivalent to a slightly supercritical Rayleigh number such that

$$\Delta = \Delta_0, \quad q = q_0, \quad C = C_0, \tag{3.1}$$

is assumed to exist initially. At $t = 0$ the temperature difference between the horizontal surfaces is raised by a non-dimensional amount $18\pi^2 L^{-1}\Delta_B$. When $t = O(1)$ the basic (i.e. externally generated) temperature field measured from zero at the lower surface can then be expressed as

$$\theta = -(R_0 + 18\pi^2(\Delta_0 + \Delta_B)\, L^{-1})\, z + 18\pi^2 \Delta_B\, L^{-1}\theta_B(z, t), \tag{3.2}$$

where, from (2.1), θ_B satisfies

$$\theta_{B_{zz}} = \theta_{B_t}, \quad \theta_B(0, t) = \theta_B(1, t) = 0, \quad \theta_B(z, 0) = z. \tag{3.3}$$

The solution of this linear system is easily determined, and, as $t \to \infty$, $\theta_B \to 0$ so that

the basic temperature field (3.2) adjusts to the form appropriate to a new value of the Rayleigh number such that

$$\Delta = \Delta_0 + \Delta_B = \Delta_1, \quad \text{say.} \tag{3.4}$$

Meanwhile, the cellular motion remains unaffected at leading order since A_{0_t}, $\tilde{A}_{0_t}$, $\tilde{A}_{1_t}$, ψ_{0_t} must all be zero, and so the solutions (2.11), (2.14), (2.15) and (2.22) all remain unchanged when $t = O(1)$.

The evolution of the base state modelled by (3.3) could be generalized to incorporate more gradual changes in external conditions on the timescale t, or changes that might invoke minor contributions to the velocity field, but the main conclusion that there can be no significant change in the cellular motion during this period still stands.

4. Adjustment in convective amplitude: $t = O(L)$

The first significant effect on the cellular motion occurs when $t = O(L)$, and it is appropriate to define a long timescale $\tilde{\tau}$ by

$$t = \frac{1+P}{4P} L\tilde{\tau}, \tag{4.1}$$

the factor involving the Prandtl number being included for convenience. This timescale is, of course, suggested by the fact that the linear growth rate of disturbances near R_0 is of order $R - R_0$, i.e. of order L^{-1}.

The core solution is now given by (2.10), but in which we now suppose $A_0 = A_0(X, \tilde{\tau})$. The equation for A_0 obtained at order $L^{-\frac{3}{2}}$ after substitution of (2.10) into (2.1) (in which $R = R_0 + 18\pi^2 L^{-1}\Delta_1$) is

$$A_{0_{\tilde{\tau}}} = \Delta_1 A_0 - A_0 |A_0|^2. \tag{4.2}$$

The initial condition at $\tilde{\tau} = 0$ is, from (2.11),

$$A_0 = \Delta_0^{\frac{1}{2}} e^{i\phi_0(X)}, \quad \phi_0 = q_0 X + C_0, \tag{4.3}$$

and so the required solution is

$$A_0 = \frac{(\Delta_0 \Delta_1)^{\frac{1}{2}} e^{\Delta_1 \tilde{\tau} + i\phi_0(X)}}{(\Delta_1 - \Delta_0 + \Delta_0 e^{2\Delta_1 \tilde{\tau}})^{\frac{1}{2}}}. \tag{4.4}$$

Thus

$$A_0 \to \Delta_1^{\frac{1}{2}} e^{i\phi_0(X)} \quad \text{as} \quad \tilde{\tau} \to \infty, \tag{4.5}$$

representing an adjustment in the amplitude of the convective flow to the value appropriate to the new Rayleigh number. Note that the roll pattern itself is unchanged since the complex argument of A_0 is always $\phi_0(X)$. This is because diffusive effects in the Bénard problem occur at a lengthscale $x \sim t^{\frac{1}{2}}$ and so the timescale $t = O(L)$ is too short for these to affect the core equation (4.2). Diffusion, as we shall see below, is limited to the boundary-layer lengthscale when $t = O(L)$, and the effect of the lateral walls can only penetrate into the core, where $x = O(L)$ (and thereby change the roll pattern) when $t = O(L^2)$.

In the boundary-layer region where $\tilde{X} = O(1)$ the solution on the timescale $\tilde{\tau}$ is given by (2.13), but in which we now suppose $\tilde{A}_{0,1} = \tilde{A}_{0,1}(\tilde{X}, \tilde{\tau})$. The equations for $\tilde{A}_0$ and $\tilde{A}_1$ are found at order $L^{-\frac{3}{2}}$ and L^{-2} after substitution of (2.13) into the governing equations (2.1). They are

$$\tilde{A}_{0_{\tilde{\tau}}} = \tilde{A}_{0_{\tilde{X}\tilde{X}}} + \Delta_1 \tilde{A}_0 - \tilde{A}_0 |\tilde{A}_0|^2 \tag{4.6}$$

and

$$\tilde{A}_{1\tilde{\tau}} = \tilde{A}_{1\tilde{X}\tilde{X}} + \Delta_1 \tilde{A}_1 - 2|\tilde{A}_0|^2 \tilde{A}_1 - \tilde{A}_0^2 \tilde{A}_1^* - \mathrm{i}\{k_1 \Delta_1 \tilde{A}_{0\tilde{X}} + k_2 \tilde{A}_{0\tilde{X}\tilde{X}\tilde{X}} - (k_3+k_4)|\tilde{A}_0|^2 \tilde{A}_{0\tilde{X}} - (k_3+k_5)\tilde{A}_0^2 \tilde{A}_{0\tilde{X}}^* - k_6 \tilde{A}_{0\tilde{X}\tilde{\tau}}\}, \quad (4.7)$$

where

$$k_6 = 8/3\sqrt{2\pi}, \quad (4.8)$$

with initial conditions at $\tilde{\tau} = 0$ given by (2.14) and (2.15). It should be noted that, strictly speaking, the solution for $\tilde{A}_1$ is first adjusted when $t = O(L^{\frac{1}{2}})$, but the adjustment is merely the addition of a term proportional to $tL^{-\frac{1}{2}}$ which matches with the $O(\tilde{\tau})$ term in $\tilde{A}_0$ as $\tilde{\tau} \to 0$, so that (2.15) remains the correct initial condition for (4.7) at $\tilde{\tau} = 0$.

The boundary conditions for (4.6) and (4.7) at $\tilde{X} = 0$ are supplied by matching with the sidewall-region solution (2.21) in which (2.22) remains valid except that a and b are now parametrically dependent upon $\tilde{\tau}$. Thus we require

$$\tilde{A}_0(0, \tilde{\tau}) = 0 \quad (4.9)$$

and, from (2.24),

$$\tilde{A}_1(0, \tilde{\tau}) = -\alpha^* \tilde{A}_{0\tilde{X}}(0, \tilde{\tau}) - \beta^* \tilde{A}_{0\tilde{X}}^*(0, \tilde{\tau}). \quad (4.10)$$

Finally, the boundary-layer solution must match with the core solution (4.4), giving

$$\tilde{A}_0 \to A_0(-1, \tilde{\tau}), \quad \tilde{A}_{1\tilde{X}} \to A_{0X}(-1, \tilde{\tau}) \quad \text{as} \quad \tilde{X} \to \infty. \quad (4.11)$$

5. The evolution of the boundary layer

In order to simplify the boundary-layer system (4.6)–(4.11) we set

$$\left.\begin{aligned} \tilde{X} &= \Delta_1^{-\frac{1}{2}} \bar{X}, \quad \tilde{\tau} = \Delta_1^{-1} \bar{\tau}, \quad \tilde{A}_0 = \Delta_1^{\frac{1}{2}} \mathrm{e}^{\mathrm{i}\phi_0(-1)} \bar{A}(\bar{X}, \bar{\tau}), \\ \tilde{A}_1 &= \Delta_1 \mathrm{e}^{\mathrm{i}\phi_0(-1)} \{\bar{A}_{\mathrm{r}}(\bar{X}, \bar{\tau}) + \mathrm{i}\bar{A}_{\mathrm{i}}(\bar{X}, \bar{\tau})\}, \end{aligned}\right\} \quad (5.1)$$

to obtain the set of real equations

$$\left.\begin{aligned} \bar{A}_{\bar{\tau}} &= \bar{A}_{\bar{X}\bar{X}} + \bar{A} - \bar{A}^3, \\ \bar{A}_{\mathrm{r}\bar{\tau}} &= \bar{A}_{\mathrm{r}\bar{X}\bar{X}} + \bar{A}_{\mathrm{r}} - 3\bar{A}^2 \bar{A}_{\mathrm{r}}, \\ \bar{A}_{\mathrm{i}\bar{\tau}} &= \bar{A}_{\mathrm{i}\bar{X}\bar{X}} + \bar{A}_{\mathrm{i}} - \bar{A}^2 \bar{A}_{\mathrm{i}} - \{k_1 \bar{A}_{\bar{X}} + k_2 \bar{A}_{\bar{X}\bar{X}\bar{X}} - (2k_3 + k_4 + k_5)\bar{A}^2 \bar{A}_{\bar{X}} - k_6 \bar{A}_{\bar{X}\bar{\tau}}\}. \end{aligned}\right\} \quad (5.2)$$

The initial conditions become

$$\bar{A}(\bar{x}, 0) = \left(\frac{\Delta_0}{\Delta_1}\right)^{\frac{1}{2}} \tanh \frac{\Delta_0^{\frac{1}{2}} \bar{X}}{\Delta_1^{\frac{1}{2}} \sqrt{2}}, \quad \bar{A}_{\mathrm{r,i}}(\bar{X}, 0) = \frac{\Delta_0}{\Delta_1} \tilde{\alpha}_{\mathrm{r,i}}\left(\frac{\Delta_0^{\frac{1}{2}} \bar{X}}{\Delta_1^{\frac{1}{2}}}\right), \quad (5.3)$$

and the boundary conditions are

$$\left.\begin{aligned} &\bar{A}(0, \bar{\tau}) = 0, \quad \bar{A}(\infty, \bar{\tau}) = \Delta_0^{\frac{1}{2}} \mathrm{e}^{\bar{\tau}} (\Delta_1 - \Delta_0 + \Delta_0 \mathrm{e}^{2\bar{\tau}})^{-\frac{1}{2}}; \\ &\bar{A}_{\mathrm{r}}(0, \bar{\tau}) = (-\alpha_{\mathrm{r}} - |\beta| \cos\{2\phi_0(-1) + \chi\}) \bar{A}_{\bar{X}}(0, \bar{\tau}), \quad \bar{A}_{\mathrm{r}\bar{X}}(\infty, \bar{\tau}) = 0; \\ &\bar{A}_{\mathrm{i}}(0, \bar{\tau}) = (\alpha_{\mathrm{i}} + |\beta| \sin\{2\phi_0(-1) + \chi\}) \bar{A}_{\bar{X}}(0, \bar{\tau}), \\ &\bar{A}_{\mathrm{i}\bar{X}}(\infty, \bar{\tau}) = \Delta_0^{\frac{1}{2}} \Delta_1^{-1} \mathrm{e}^{\bar{\tau}} (\Delta_1 - \Delta_0 + \Delta_0 \mathrm{e}^{2\bar{\tau}})^{-\frac{1}{2}} \phi_{0X}(-1). \end{aligned}\right\} \quad (5.4)$$

A more general initial-value problem can be considered in which the profile for A_0 in the core at $\tilde{\tau} = 0$ is a completely arbitrary complex function of X. A solution similar

to (4.4) can still be found, and in the boundary layer both $\bar{A}_{\mathrm{r}\bar{X}}$ and $\bar{A}_{\mathrm{i}\bar{X}}$ are then generally non-zero as $\bar{X}\to\infty$.

Possible asymptotic forms for $\bar{A}_{\mathrm{r}}$ and $\bar{A}_{\mathrm{i}}$ for large $\bar{X}$ are

$$\bar{A}_{\mathrm{r}} \sim \frac{\mathrm{e}^{\bar{\tau}}(\xi_1\bar{X}+\xi_2+\ldots)}{(\Delta_1-\Delta_0+\Delta_0\mathrm{e}^{2\bar{\tau}})^{\frac{3}{2}}}, \quad \bar{A}_{\mathrm{i}} \sim \frac{\mathrm{e}^{\bar{\tau}}(\xi_3\bar{X}+\xi_4+\ldots)}{(\Delta_1-\Delta_0+\Delta_0\mathrm{e}^{2\bar{\tau}})^{\frac{1}{2}}}, \tag{5.5}$$

where ξ_1, ξ_2, ξ_3 and ξ_4 are constants. The initial conditions (5.3) and boundary conditions (5.4) imply that these have the values

$$\xi_1=\xi_2=0, \quad \xi_3=\Delta_0^{\frac{1}{2}}\Delta_1^{-1}\phi_{0X}(-1), \quad \xi_4=\Delta_0\Delta_1^{-\frac{1}{2}}(K_1+K_2+\tilde{c}-\sqrt{2}\,\tilde{b}). \tag{5.6}$$

Although the first of the asymptotic forms (5.5) is uniformly valid for $\bar{X}\gg 1$ and all $\bar{\tau}$, we shall see below that the second is only valid for $\bar{X}\gg\bar{\tau}^{\frac{1}{2}}$ when $\bar{\tau}\gg 1$, and thus the influence of the initial core profile $\phi_0(X)$ on the flow near the wall begins to be reduced. As $\bar{\tau}\to\infty$ the boundary layer expands and allows the influence of the lateral wall to spread into the core. It is this reaction to the increase in Rayleigh number that triggers the eventual adjustment of the roll pattern throughout the container.

In order to analyse the boundary-layer structure for large $\bar{\tau}$ it is first noted that, from (5.2) and (5.4),

$$\bar{A}=\tanh\frac{\bar{X}}{\sqrt{2}}+O(\mathrm{e}^{-2\bar{\tau}}) \quad \text{as} \quad \bar{\tau}\to\infty, \tag{5.7}$$

and also that the complete solution for $\bar{A}_{\mathrm{r}}$ is

$$\bar{A}_{\mathrm{r}}=(-\alpha_{\mathrm{r}}-|\beta|\cos\{2\phi_0(-1)+\chi\})\,\bar{A}_{\bar{X}}(\bar{X},\bar{\tau}). \tag{5.8}$$

The solution for $\bar{A}_{\mathrm{i}}$ develops a double structure as $\bar{\tau}\to\infty$, consisting of an inner region where $\bar{X}=O(1)$ and an outer region where $\bar{\eta}=\bar{X}/\bar{\tau}^{\frac{1}{2}}=O(1)$. This leads to an expansion in powers of $\bar{\tau}^{\frac{1}{2}}$, and in the inner region the solution has the form

$$\begin{aligned}\bar{A}_{\mathrm{i}}=\bar{\tau}^{\frac{1}{2}}\{c_0\Theta\}+\{c_1\Theta+b_1(\bar{X}\Theta-\sqrt{2})+I(\bar{X})\}\\ +\bar{\tau}^{-\frac{1}{2}}\{c_2\Theta+b_2(\bar{X}\Theta-\sqrt{2})+c_0(\tfrac{1}{4}\bar{X}^2\Theta+\Theta-\bar{X}/\sqrt{2})\}+O(\bar{\tau}^{-1})\end{aligned} \tag{5.9}$$

as $\bar{\tau}\to\infty$, where $\Theta=\tanh(\bar{X}/\sqrt{2})$ and c_0, c_1, c_2, b_1 and b_2 are arbitrary constants. The leading term of order $\bar{\tau}^{\frac{1}{2}}$ is made necessary by the form of the outer solution and also generates the particular solution involving c_0 at order $\bar{\tau}^{-\frac{1}{2}}$ via the time-derivative term $\bar{A}_{\mathrm{i}\bar{\tau}}$ in (5.2). The constants b_1 and b_2 are determined by the boundary condition (5.4) at $\bar{X}=0$ as

$$b_1=-\tfrac{1}{2}(\alpha_0+|\beta|\sin\{2\phi_0(-1)+\chi\})=\tilde{b}=q_0\Delta_0^{-1}, \quad b_2=0, \tag{5.10}$$

and then, for $\bar{X}\gg 1$,

$$\bar{A}_{\mathrm{i}}\sim\bar{\tau}^{\frac{1}{2}}c_0+\{b_1\bar{X}+c_1-\sqrt{2}\,b_1+K_1+K_2\}+\bar{\tau}^{-\frac{1}{2}}\{\tfrac{1}{4}c_0\bar{X}^2-c_0\bar{X}/\sqrt{2}+c_0+c_2\}. \tag{5.11}$$

In the outer region the time derivative $\bar{A}_{\mathrm{i}\bar{\tau}}$ must balance at leading order, and since $\bar{A}\sim 1$ in this region,

$$\bar{A}_{\mathrm{i}}=\bar{\tau}^{\frac{1}{2}}G_0(\bar{\eta})+G_1(\bar{\eta})+O(\bar{\tau}^{-\frac{1}{2}}), \tag{5.12}$$

where

$$G_0''+\tfrac{1}{2}\bar{\eta}G_0'-\tfrac{1}{2}G_0=0, \tag{5.13}$$

$$G_1''+\tfrac{1}{2}\bar{\eta}G_1'=0. \tag{5.14}$$

The general solutions are

$$G_0=p_0\bar{\eta}+p_1\{2\pi^{-\frac{1}{2}}\mathrm{e}^{-\frac{1}{4}\bar{\eta}^2}-\bar{\eta}(1-\mathrm{erf}[\tfrac{1}{2}\bar{\eta}])\}, \tag{5.15}$$

$$G_1=p_2+p_3\{1-\mathrm{erf}[\tfrac{1}{2}\bar{\eta}]\}. \tag{5.16}$$

Now (5.5) requires that

$$\left.\begin{aligned} G_0 &\sim \Delta_1^{-1} q_0 \bar{\eta} + 0, \\ G_1 &\sim \Delta_0^{\frac{1}{2}} \Delta_1^{-\frac{1}{2}} (K_1 + K_2 + \tilde{c} - \sqrt{2}\,\tilde{b}), \end{aligned}\right\} \quad (\bar{\eta} \to \infty), \tag{5.17}$$

giving

$$p_0 = \Delta_1^{-1} q_0, \quad p_2 = \Delta_0^{\frac{1}{2}} \Delta_1^{-\frac{1}{2}} (K_1 + K_2 + \tilde{c} - \sqrt{2}\,\Delta_0^{-1} q_0). \tag{5.18}$$

The solutions (5.15) and (5.16) must also match with the inner form (5.11), which requires that

$$\left.\begin{aligned} G_0 &\sim c_0 + b_1 \bar{\eta} + \tfrac{1}{4} c_0 \bar{\eta}^2, \\ G_1 &\sim c_1 - \sqrt{2} b_1 + K_1 + K_2 - c_0 \bar{\eta}/\sqrt{2}, \end{aligned}\right\} \quad (\bar{\eta} \to 0), \tag{5.19}$$

and so

$$\left.\begin{aligned} c_0 = \frac{2p_1}{\pi^{\frac{1}{2}}}, \quad b_1 &= p_0 - p_1, \\ c_1 - \sqrt{2}\, b_1 + K_1 + K_2 = p_2 + p_3, \quad -\frac{c_0}{\sqrt{2}} &= -\frac{p_3}{\pi^{\frac{1}{2}}}. \end{aligned}\right\} \tag{5.20}$$

This fixes the unknown constants p_1 and p_3 in the outer solution and c_0 and c_1 in the inner solution as

$$\left.\begin{aligned} p_1 = \frac{p_3}{\sqrt{2}} = \tfrac{1}{2} c_0 \pi^{\frac{1}{2}} &= \frac{q_0(\Delta_0 - \Delta_1)}{\Delta_0 \Delta_1}, \\ c_1 &= \Delta_0^{\frac{1}{2}} \Delta_1^{-\frac{1}{2}} \tilde{c} + (\Delta_0^{\frac{1}{2}} \Delta_1^{-\frac{1}{2}} - 1)(K_1 + K_2 + \sqrt{2}\, q_0 \Delta_0^{-\frac{1}{2}} \Delta_1^{-\frac{1}{2}}), \end{aligned}\right\} \tag{5.21}$$

and completes the solution to terms of order 1 in each region. The leading terms are

$$\bar{A}_i \sim \frac{2 q_0 \bar{\tau}^{\frac{1}{2}}}{\pi^{\frac{1}{2}} \Delta_1} \left(1 - \frac{\Delta_1}{\Delta_0}\right) \tanh \frac{\bar{X}}{\sqrt{2}}, \quad \bar{X} = O(1), \tag{5.22}$$

$$\bar{A}_i \sim \frac{q_0 \bar{\tau}^{\frac{1}{2}}}{\Delta_1} \left\{ \bar{\eta} + \left(1 - \frac{\Delta_1}{\Delta_0}\right) \left[\frac{2}{\pi^{\frac{1}{2}}} e^{-\frac{1}{4}\bar{\eta}^2} - \bar{\eta} \left(1 - \operatorname{erf} \frac{\bar{\eta}}{2}\right) \right] \right\}, \quad \bar{X} = O(\bar{\tau}^{\frac{1}{2}}). \tag{5.23}$$

A numerical solution of the system (5.2)–(5.4) was undertaken to confirm the above structure, and the results are shown in figure 3. Although the value of $\tilde{c}$ is unknown its contribution to the solution for $\bar{A}_i$ is

$$\bar{A}_i = \tilde{c} \Delta_0^{\frac{1}{2}} \Delta_1^{-\frac{1}{2}} \bar{A}(\bar{X}, \bar{\tau}), \tag{5.24}$$

and this portion can simply be excluded from the numerical solution by setting $\tilde{c} = 0$. The various parameters used in the solution correspond to a semi-aspect ratio $L = 5$ and a Prandtl number $P = 0.2$ as featured in figure 2. The initial and final values of the Rayleigh number are taken as $\Delta_0 = 0.33$ and $\Delta_1 = 4.55$ and the initial state has $q_0 = -\frac{1}{2}$ and $C_0 = 0$. The value of $\tilde{b}$ is -1.52. The numerical method of solution was based on forward differences in $\bar{\tau}$ and centred differences in $\bar{X}$, and the results shown in figure 3 are for step lengths of 0.005 and 0.2 (respectively) with an outer boundary at $\bar{X} = 16$.

The main features of the asymptotic results are adequately reproduced, including the double structure of the solution for $\bar{A}_i$ as $\bar{\tau} \to \infty$. In the inner zone the development of the hyperbolic-tangent profile (5.22) can be observed attaining its maximum value ($\sim 1.59 \bar{\tau}^{\frac{1}{2}}$) at the edge of the zone. Outside this the error-function profile (5.23) takes over and adjusts the gradient $\bar{A}_{i\bar{X}}$ from the value $q_0 \Delta_0^{-1} \approx -1.52$ to the value $q_0 \Delta_1^{-1} \approx -0.11$ at the expanding edge of the layer. In terms of the overall amplitude function, this is equivalent to an adjustment of the gradient of the phase function

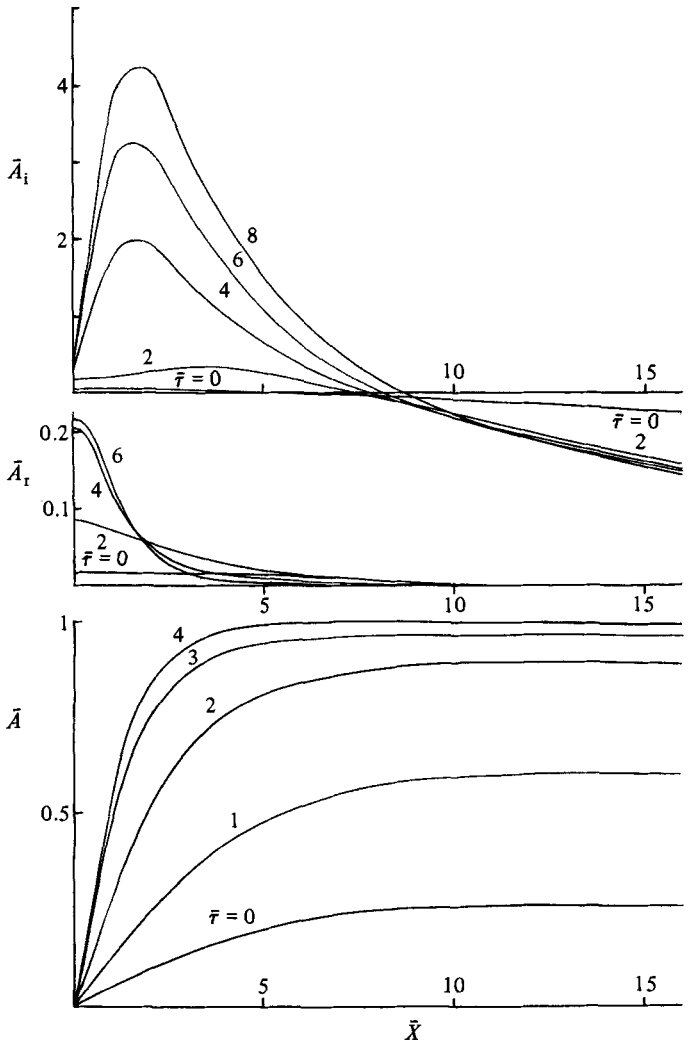

FIGURE 3. Boundary-layer evolution. Numerical solution of (5.2)–(5.4) showing profiles of $\bar{A}$, $\bar{A}_r$ and $\bar{A}_i$ as functions of $\bar{X}$ at various values of $\bar{\tau}$. See text for values of the various parameters.

from a value $q_0 \Delta_1/\Delta_0$ associated with the relative change in Rayleigh number, Δ_1/Δ_0, to the value q_0 associated with the initial core profile; in between, the form (5.23) is the embryo of the new core solution and represents the first significant modification to the roll pattern. As the outer zone of the boundary layer spreads, it eventually becomes comparable in size to the core, and the asymptotic structure for $\tilde{\tau} = O(1)$ must be revised. The boundary layer is expanding such that $\tilde{X} \sim \tilde{\tau}^{\frac{1}{2}}$ or $x \sim L^{\frac{1}{2}}\tilde{\tau}^{\frac{1}{2}}$, and this is comparable to the horizontal scale of the core when $\tilde{\tau} \sim L$. Also, the solution for $\bar{A}_i$ is of order $\tilde{\tau}^{\frac{1}{2}}$, while that for $\bar{A}$ is of order one, again suggesting breakdown when $\tilde{\tau} \sim L$. This breakdown heralds the onset of the final evolutionary stage when $t = O(L^2)$ and the roll pattern is adjusted to its new form.

6. Evolution of the roll pattern: $t = O(L^2)$

We define a timescale τ as

$$t = \frac{1+P}{4P} L^2 \tau, \tag{6.1}$$

as suggested by the analysis of §5, and in the core the solution is given by (2.10) but now with

$$A_0 = \Delta_1^{\frac{1}{2}} e^{i\phi(X,\tau)}. \tag{6.2}$$

Substitution of (2.10) into the governing equations (2.1) and consideration of terms to order $L^{-\frac{5}{2}}$ shows that ϕ satisfies the diffusion equation

$$\phi_\tau = \phi_{XX}. \tag{6.3}$$

In view of (4.5) the initial condition for this equation is

$$\phi = \phi_0(X) = q_0 X + C_0 \tag{6.4}$$

at $\tau = 0$.

In the boundary layer at $X = -1$ the long timescale (6.1) relegates all the time derivatives in (4.6) and (4.7) to higher order, and so τ appears only parametrically in the solutions. The required solution for $\tilde{A}_0$ that matches with (6.2) and the initial form (5.7) is therefore

$$\tilde{A}_0 = \Delta_1^{\frac{1}{2}} \tanh\left(\frac{\Delta_1^{\frac{1}{2}} \tilde{X}}{\sqrt{2}}\right) e^{i\phi(-1,\tau)}, \tag{6.5}$$

while the solution for $\tilde{A}_1$ is

$$\tilde{A}_1 = \Delta_1 \{\tilde{\alpha}_r(\Delta_1^{\frac{1}{2}} \tilde{X}) + i\tilde{\alpha}_i(\Delta_1^{\frac{1}{2}} \tilde{X})\} e^{i\phi(-1,\tau)}, \tag{6.6}$$

where the coefficients $\tilde{a}$, $\tilde{b}$ and $\tilde{c}$ are parametrically dependent upon τ. $\tilde{A}_0$ and $\tilde{A}_1$ are still related by the condition (4.10), and so, in particular,

$$\tilde{b} = -\tfrac{1}{2}(\alpha_0 + |\beta| \sin\{2\phi(-1,\tau) + \chi\}). \tag{6.7}$$

Now $\tilde{A}_1 \sim i\Delta_1^{\frac{3}{2}} \tilde{b} \tilde{X} e^{i\phi(-1,\tau)}$ as $\tilde{X} \to \infty$, and this matches with the core solution (6.2) if

$$\phi_X(-1,\tau) = \Delta_1 \tilde{b} = -\tfrac{1}{2}\Delta_1(\alpha_0 + |\beta| \sin\{2\phi(-1,\tau) + \chi\}). \tag{6.8}$$

From a similar consideration of the boundary layer at $X = 1$,

$$\phi_X(1,\tau) = -\tfrac{1}{2}\Delta_1(\alpha_0 - |\beta| \sin\{2\phi(1,\tau) - \chi\}). \tag{6.9}$$

Thus the new roll pattern must be found as the final steady-state solution of (6.3) specified by the original roll pattern and the boundary conditions (6.8) and (6.9) imposed by the interaction with the sidewalls. These conditions actually provoke the evolution, and it should be noted that the initial singularities at $X = \pm 1$ inferred by (6.8), (6.9) and (6.4) correspond to the outer zones of the double-structured boundary layers described in §5. Thus the singularities are smoothed out during the period when $\tilde{\tau} = O(1)$. Further discussion of the initial development of the system at $\tau = 0$ is given in Appendix A.

Numerical solutions of the system (6.3), (6.4), (6.8) and (6.9) were found using a finite-difference scheme that handled the nonlinearity in the boundary conditions by a Newton iteration. The scheme used ϕ and $s = \phi_X$ as independent variables, and then the first-order system

$$\phi_\tau = s_X, \quad s = \phi_X \tag{6.10}$$

was discretized using central differences in both X and τ. The resulting set of boundary conditions and equations was linearized by applying a Newton iteration, and the evaluation of the increments required the solution of a five-band matrix equation. The iteration was usually required to converge to within a tolerance of 10^{-6}, and this was generally achieved within two or three iterations for a time step of 0.01 and taking the solution at the previous time step as initial guess. No special treatment of the initial discontinuity in gradient at $\tau = 0, X = \pm 1$ was used; this never affected convergence and variations in the size of both the space and time steps suggested only minor loss of accuracy from this source. Step lengths in the X-direction were normally taken as either 0.1 or 0.02. Final convergence of the scheme to steady state is easily tested by the form of s, which must approach a constant value across the container.

7. Fundamental properties of the final stage of evolution

Before presenting the numerical results it is useful to outline some of the basic properties of the system (6.3), (6.4), (6.8), (6.9) governing the final evolution. To summarize the results of §6, the roll pattern is determined by the phase function $\phi(X,\tau)$, which satisfies

$$\left.\begin{aligned} \phi_\tau &= \phi_{XX} \quad (-1 \leqslant X \leqslant 1,\ \tau \geqslant 0), \\ \phi(X,0) &= \phi_0(X) = q_0 X + C_0, \\ \phi_X(\pm 1,\tau) &= -\tfrac{1}{2}\Delta(\alpha_0 \mp |\beta| \sin\{2\phi(\pm 1,\tau) \mp \chi\}), \end{aligned}\right\} \tag{7.1}$$

where q_0 and C_0 are fixed by the initial configuration and Δ is a measure of the new Rayleigh number (i.e. $\Delta = \Delta_1$ in the notation of §§3–6).

7.1. *Steady states*

These are possible when ϕ has the form

$$\phi = qX + C, \tag{7.2}$$

and it is easily shown from (7.1) that this requires either

$$2q = -\Delta(\alpha_0 - (-1)^n |\beta| \sin(2q-\chi)), \quad C = \tfrac{1}{2}n\pi \quad (n \text{ integer}) \quad \text{(class I solution)} \tag{7.3}$$

or

$$2q = \chi - \tfrac{1}{2}\pi + m\pi \quad (m \text{ integer}) \quad \text{(class II solution)}, \tag{7.4}$$

consistent with the results (2.30) and (2.31) above (see also figures 1 and 2).

7.2. *Stability*

The stability of these states has been discussed by Daniels (1981) by considering the evolution of a perturbation to (7.2). The main results may be summarized as follows. First, all of the class II solutions are unstable. Of the class I solutions, the ones for which

$$\Delta(-1)^n |\beta| \cos(2q-\chi) < 0, \tag{7.5}$$

i.e. {gradient of right-hand side of (7.3) as a function of $2q$} < 0, are stable. Although the other class I solutions are all unstable, it is important to note that their destabilization is crucially dependent upon whether the disturbance to ϕ in (7.2) is even or odd about $X = 0$. Even disturbances are most dangerous and destabilize all

solutions that do not satisfy (7.5). However, odd disturbances only destabilize those solutions for which

$$\Delta(-1)^n|\beta|\cos(2q-\chi) > 1, \tag{7.6}$$

which, in terms of the graphical constructions of figures 1 and 2, can usefully be expressed as

$$\left\{\begin{array}{l}\text{gradient of right-hand side of (7.3)}\\ \text{as a function of } 2q\end{array}\right\} > \left\{\begin{array}{l}\text{gradient of left-hand side of (7.3)}\\ \text{as a function of } 2q\end{array}\right\}. \tag{7.7}$$

These two sides are equal at points of tangency of the straight line and sinusoidal constructions representing the two sides of (7.3) in figures 1 and 2, and are the points at which new pairs of steady-state phase-winding solutions exist (or cease to exist) as a function of the Rayleigh number. In contrast, the true points of neutral stability (i.e. when even disturbances are allowed) are those at which the left-hand side of (7.5) is zero, and these are the points at which the class II solutions bifurcate from the class I solutions. In figures 1 and 2 the stable and unstable solutions satisfying (7.5) and (7.6) respectively are shown by heavy and light lines. The unstable solutions that are destabilized only by even disturbances are shown by dotted lines.

7.3. *Preservation of even and odd solutions*

A fundamental property of the system (7.1) is the preservation of an even or odd solution with time (i.e. a solution for ϕ for which the resulting flow pattern is either even or odd about $X = 0$). This can be seen by writing

$$\phi = \phi^{\mathrm{E}} + \phi^{\mathrm{O}}, \tag{7.8}$$

where ϕ^{E} and ϕ^{O} are the even and odd parts of ϕ. Substitution into (7.1) shows that

$$\phi_\tau^{\mathrm{E,O}} = \phi_{XX}^{\mathrm{E,O}}, \tag{7.9}$$

$$\phi_X^{\mathrm{E}}(-1,\tau) = -\tfrac{1}{2}\Delta|\beta|\cos\{2\phi^{\mathrm{O}}(-1,\tau)+\chi\}\sin\{2\phi^{\mathrm{E}}(-1,\tau)\}, \tag{7.10}$$

$$\phi_X^{\mathrm{O}}(-1,\tau) = -\tfrac{1}{2}\Delta(\alpha_0+|\beta|\sin\{2\phi^{\mathrm{O}}(-1,\tau)+\chi\}\cos\{2\phi^{\mathrm{E}}(-1,\tau)\}, \tag{7.11}$$

from which it can be seen that possible solutions for ϕ^{E} for *all* time are $\phi^{\mathrm{E}} = \frac{1}{2}n\pi$, where n is an integer. ϕ^{O} is then determined using (7.11). Thus if the initial configuration is one of the steady-state solutions in which $\phi^{\mathrm{E}}(X,0) = C_0 = \frac{1}{2}n\pi$ the solution for ϕ^{E} will retain this form for all $\tau > 0$, and it follows from (6.2) and (2.10) that the flow pattern remains either even or odd throughout the entire evolution. This implies that the solution can actually evolve to an unstable state (see the numerical study below) if no perturbation to the even part of ϕ occurs during the evolution; the change in the value of Δ necessitates a change in the value of q, but this is effectively a perturbation to only the odd part of the final solution for ϕ. Thus the system does not differentiate between the dotted and heavy sections of the curves in figures 1 and 2, with the result that the roll pattern can adjust to an unstable state on one of the dotted sections.

In practice, physical conditions might be expected to introduce a disturbance which would lead to a contribution to the even part of ϕ, and then the full stability criterion (7.5) must come into effect and drive the system to a stable configuration. For example, suppose that initially

$$\phi^{\mathrm{E}} = \tfrac{1}{2}n\pi + \bar{\epsilon}\bar{\phi}(X) \quad (\bar{\epsilon} \ll 1), \tag{7.12}$$

representing a small perturbation of order $\bar{\epsilon}$ to the even part of ϕ. Then when $\tau = O(1)$ the solution can be expanded in powers of $\bar{\epsilon}$:

$$\phi^{\mathrm{O}} = \bar{\phi}^{\mathrm{O}} + \ldots, \quad \phi^{\mathrm{E}} = \tfrac{1}{2}n\pi + \bar{\epsilon}\bar{\phi}^{\mathrm{E}} + \ldots, \tag{7.13}$$

and from (7.10) and (7.11), $\bar{\phi}^{\mathrm{O}}$ and $\bar{\phi}^{\mathrm{E}}$ satisfy

$$\left.\begin{aligned} \bar{\phi}^{\mathrm{O,E}}_{\tau} = \bar{\phi}^{\mathrm{O,E}}_{XX}, \quad \bar{\phi}^{\mathrm{E}}_{X}(-1,\tau) &= -\Delta\,|\beta|(-1)^n\,\bar{\phi}^{\mathrm{E}}(-1,\tau)\cos\{2\bar{\phi}^{\mathrm{O}}(-1,\tau)+\chi\}, \\ \bar{\phi}^{\mathrm{O}}_{X}(-1,\tau) &= -\tfrac{1}{2}\Delta(\alpha_0 + |\beta|\,(-1)^n \sin\{2\bar{\phi}^{\mathrm{O}}(-1,\tau)+\chi\}). \end{aligned}\right\} \tag{7.14}$$

As $\tau \to \infty$ it can be expected that $\bar{\phi}^{\mathrm{O}} \to \bar{q}X$, where

$$\bar{q} = -\tfrac{1}{2}\Delta(\alpha_0 + |\beta|(-1)^n \sin\{\chi - 2\bar{q}\}), \tag{7.15}$$

and these values of $\bar{q}$ and n will correspond to a solution on either the heavy or dotted portions of the curves in figures 1 and 2, the evolution of $\bar{\phi}^{\mathrm{O}}$ being subject to the stability criterion (7.6). The new roll pattern at this stage is approximately the one that would be established if no perturbation to the even part of ϕ were introduced into the system. However, assuming a non-zero perturbation in (7.12) the solution for $\bar{\phi}^{\mathrm{E}}$ will have the form

$$\bar{\phi}^{\mathrm{E}} \sim \Phi(X)\,\mathrm{e}^{k\tau} \tag{7.16}$$

as $\tau \to \infty$, where

$$\Phi'' - k\Phi = 0, \quad \Phi'(-1) = -\Delta\,|\beta|(-1)^n\,\Phi(-1)\cos(2\bar{q} - \chi), \tag{7.17}$$

and k takes its maximum value. The precise form of Φ will depend on the initial disturbance $\bar{\phi}(X)$, but it is clear from (7.17) that in general

$$\Phi \propto \cosh k^{\frac{1}{2}}X, \tag{7.18}$$

where

$$k^{\frac{1}{2}}\tanh k^{\frac{1}{2}} = \Delta|\beta|(-1)^n\cos(2\bar{q} - \chi). \tag{7.19}$$

Thus the maximum value of k is positive if and only if $|\beta|\,(-1)^n\cos(2\bar{q} - \chi) > 0$. This is consistent with the stability criterion (7.5): if $\bar{q}$ and n are such that the solution is close to a stable state as $\tau \to \infty$ then the maximum value of k is negative, the solution (7.16) decays to zero and the final state is the one in which $q = \bar{q}$. Conversely, if $\bar{q}$ and n are such that the solution is close to an unstable state as $\tau \to \infty$, the maximum value of k is positive and the solution (7.16) grows until the expansion (7.13) fails when $\tau \sim k^{-1}\,|\ln\bar{\epsilon}|$. Both ϕ^{O} and $\phi^{\mathrm{E}} - \frac{1}{2}n\pi$ are then order one, and a second stage of evolution to a new roll pattern with a value of q different from $\bar{q}$ and a new value of n will occur.

This is perhaps the most interesting property of the evolutionary system, since it demonstrates that, in some circumstances it is not really sufficient to consider simply the 'natural evolution' of the roll pattern due to the change in Rayleigh number. Arbitrarily small external disturbances can play a crucial role in determining the complete evolution and may, as in the analysis of (7.12)–(7.19), lead to a situation in which a new roll pattern is almost established owing to the natural evolution, but is then modified again by external disturbances. The final state could then depend on the precise way in which the perturbation (7.12) is triggered, with a centred disturbance presumably equivalent, in some sense, to a non-zero value of $\bar{\phi}$ at a single value of X. These considerations could have an important bearing on experimental observations, and of course the significance and size of external effects may differ from experiment to experiment. In the present analysis it is assumed that the natural evolution is of primary significance and it seems likely that this would generally be the case. If sufficiently large and widespread external disturbances were allowed there would of course be no reason for the flow to follow the evolutionary pattern described in the present work.

8. Numerical results

The numerical experiments were designed to test the properties outlined in the previous section and to study the evolution in situations where multiple stable states exist at the new Rayleigh number. In most cases the initial configuration was taken to be that which would be expected to occur when the Rayleigh number just exceeds its critical value so that the solution is either even or odd ($C = 0, \pi$ or $C = \frac{1}{2}\pi, \frac{3}{2}\pi$) and there is no phase winding ($q_0 = \phi_{0X} = 0$). These four states are labelled A and B in figures 1 and 2, where the steady-state solutions for Prandtl numbers $P = 10$ and $P = 0.2$ (respectively) are displayed. In both cases the value of χ is chosen to correspond to a semi-aspect ratio $L = 5$, which means that the two odd solutions (at A) are stable and the two even solutions (at B) are unstable. The class II solutions correspond to points of intersection on the vertical lines in the figures, are entirely unstable, and so of relatively minor significance. The class I solutions correspond to points of intersection on the sinusoidal curves and their stability characteristics are labelled according to the results (7.5) and (7.7). Each stable section of these curves is associated with a fixed number of rolls, as labelled and given roughly by the formula (1.7); each transition between a state with n rolls and one with $n+2$ rolls (which can only be ascertained by calculation of the sidewall solution (2.21)) occurs at a point on the unstable section of the curve (Daniels 1981).

The two situations shown in figures 1 and 2 are chosen to represent the two distinct types of behaviour that can occur as the local Rayleigh number Δ is increased from zero. In figure 1 the system can change by a relatively small amount as the value of Δ increases, with a stable steady-state solution of 7 rolls always available on the section AC. In contrast, in figure 2 the number of rolls must continually decrease as the value of Δ is raised; of course with $L = 5$ the assumptions on which the theory is based (namely $L \gg 1$ and $R - R_0 = O(L^{-1})$) are effectively violated, and this is reflected by the fact that the number of rolls must eventually decrease to one in this case. In reality only the value of χ is needed to produce figure 2, and so L can in fact be taken as any value that satisfies (2.26). With $L = 5$ the results remain physically realistic provided that Δ is not too large, and this particular value of L is selected merely to provide an idea of the overall flow pattern in a specific case (see figures 5, 7 and 9 below).

The results pertaining to the steady states of figure 1 are first described. The numerical scheme was tested by starting from the initial profile

$$\phi(X, 0) = \phi_0(X) = q_0 X + C_0 \quad \text{with} \quad q_0 = 0, \quad C_0 = \tfrac{1}{2}\pi, \tag{8.1}$$

which is one of the two stable solutions at A. The value of Δ was set at 0.5 in (7.1) and the solution smoothly evolved to the final state

$$\phi(X, \infty) = q_1 X + C, \quad \text{with} \quad q_1 = 0.05, \quad C_1 = \tfrac{1}{2}\pi, \tag{8.2}$$

which corresponds to the point D in figure 1. The value of $\phi(0, \tau)$ remained at $\frac{1}{2}\pi$ throughout the evolution and $\phi_X(X, \tau)$ remained an even function of X, confirming the predictions of §7.3 that if the initial configuration is that of an odd (or even) solution it will remain so for all time. A second run with the same initial conditions but with $\Delta = 5$ resulted in a similar transition but terminating with $q_1 = 0.21, C_1 = \frac{1}{2}\pi$ corresponding to the point E in figure 1. The third run was started from the unstable (even) state at B with $\Delta = 0.5$ and

$$q_0 = 0, \quad C_0 = 0, \tag{8.3}$$

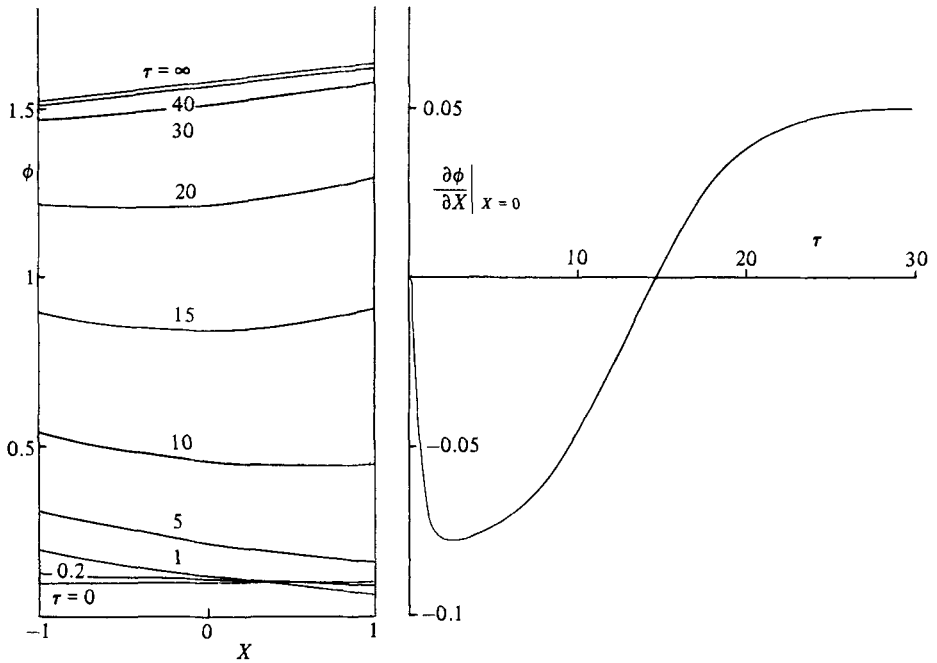

FIGURE 4. Properties of the solution $\phi(X,\tau)$ for the transition from the state (8.4) near B in figure 1 to the stable state at D.

and this evolved to $q_1 = -0.1$, $C_1 = 0$, the solution remaining even throughout the evolution. Of course this means that the solution has evolved to an unstable state (the point F in figure 1). The reason is that the steady-state solution at F is only destabilized by the even part of a disturbance to ϕ, and if (8.3) is regarded as a perturbation to the final state q_1, C_1 it is seen that no such component is present. In practice, either through rounding errors in the computations or possibly small disturbances in experiments, the solution would eventually diverge from this state on a timescale depending on the size of the disturbance. This was confirmed by replacing the initial profile (8.3) by

$$q_0 = 0, \quad C_0 = 0.1. \tag{8.4}$$

The slightly non-zero value of C_0 now causes the solution to diverge from the point F (although its initial tendency is to approach that solution) and a second stage of evolution over a long timescale accomplishes the eventual transition to the stable state at D. The two stages are clearly shown in figure 4, and the results are consistent with an analytic solution for small A described in Appendix B.

Figure 5 shows the streamline patterns at various stages during the evolution from the approximately even state (8.4) to the odd state at D. These are constructed from a composite expression for ψ that coincides with the leading terms of the formal asymptotic expansions in each of the three zones of the container. For $x < 0$ it is

$$\psi = -\frac{8}{\pi}\left\{\epsilon^{\frac{1}{2}}\sin\left[\phi(X,\tau)+\frac{\pi x}{\sqrt{2}}\right]\tanh\frac{\bar{X}}{\sqrt{2}}+\epsilon\left(\left[b_r\sin\frac{\pi x}{\sqrt{2}}+b_i\cos\frac{\pi x}{\sqrt{2}}\right]e^{-\bar{X}}+\tfrac{1}{2}de^{-2\pi x_1}\right)\right\}$$
$$\times\sin\pi z, \tag{8.5}$$

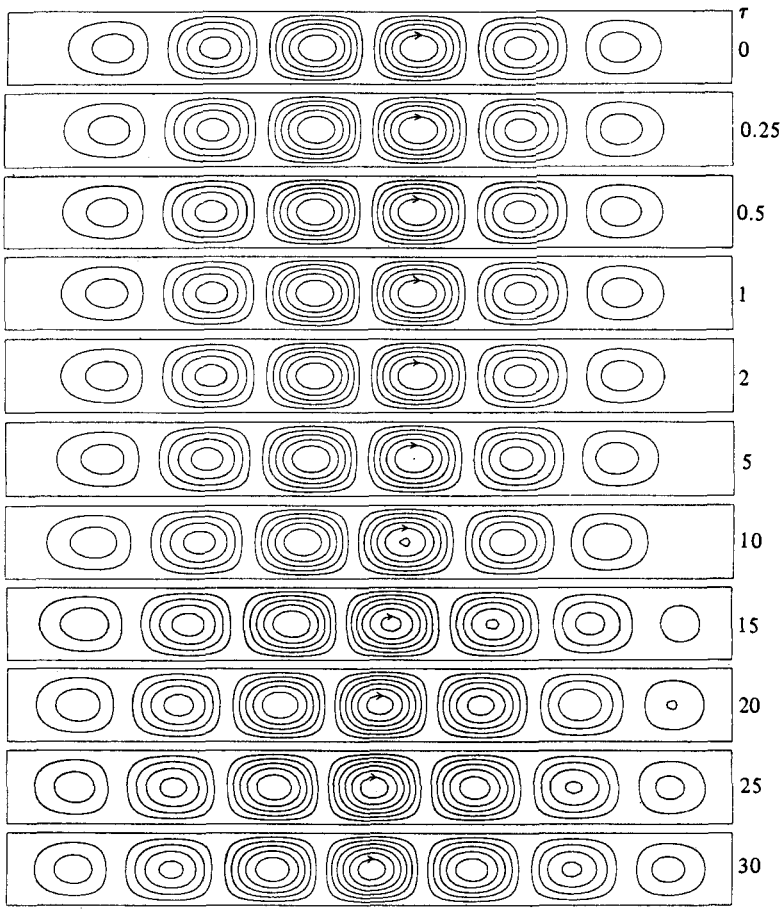

FIGURE 5. Streamline patterns at intervals of 0.1 for various values of τ for the transition of figure 4.

where x_1, $\bar{X}$ and X are as defined in §§2 and 5, $\epsilon = \Delta L^{-1}$, and d and $b = b_r + ib_i$ are given by (2.24) and (2.27) in which $a = e^{i\phi(-1,\tau)}/\sqrt{2}$. A similar formula is used for $x > 0$. Because of the long timescale of the motion, the streamlines are approximate particle paths.

The results pertaining to the steady-state solutions of figure 2 are now described. A number of results were obtained for $\Delta = 4.545$, where there are six stable solutions available (at C, D, E in figure 2), four of which are even and two odd. There are also two unstable class I even solutions at F. The first run started from an initial configuration at the stable odd solution at A with $q_0 = 0$, $C_0 = \frac{1}{2}\pi$. The solution remained odd and evolved to the stable solution at D, as shown in figure 6, with

$$q_1 = -5.95, \quad C_1 = \tfrac{1}{2}\pi. \tag{8.6}$$

This is in fact the only possibility, since the solution must remain odd and D is the only available odd solution at $\Delta = 4.545$. One of the even solutions can only be attained if the initial configuration has $C_0 \neq \frac{1}{2}\pi, \frac{3}{2}\pi$, and a summary of some experiments with different values of C_0 is given in table 1. In all cases in which the solution converged to an even final state, the state which required the minimum change in q (i.e. the minimum decrease in the number of rolls) was selected; this was

Initial state		Final state $\Delta = 4.545$	
q_0	C_0	q_1	C_1
0	$-\frac{1}{4}\pi$	−5.95	$-\frac{1}{2}\pi$
0	0	−5.00	0
0	0.1	−5.00	0
0	$\frac{1}{4}\pi$	−5.95	$\frac{1}{2}\pi$
0	$\frac{1}{2}\pi-0.1$	−5.95	$\frac{1}{2}\pi$
0	$\frac{1}{2}\pi$	−5.95	$\frac{1}{2}\pi$

TABLE 1

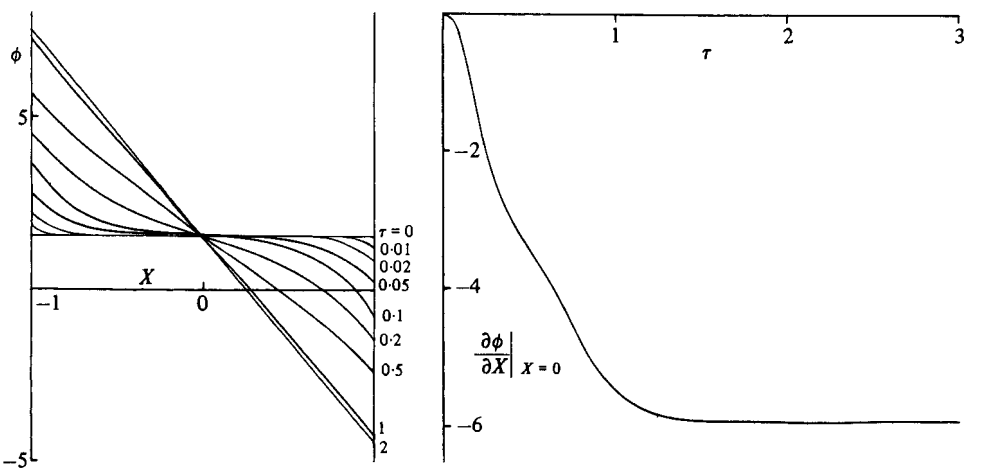

FIGURE 6. Properties of the solution $\phi(X,\tau)$ for the transition from A in figure 2 to the stale state at D.

the stable state at C, where $q_1 = -5.0$. The unstable state at F should never be selected since it can be destabilized by either even or odd perturbations and the difference in the values of q_0 and q_1 is effectively an odd perturbation of the solution at F. The stable even state at E is probably only attainable following a decrease in the Rayleigh number. The roll-pattern evolution for the transition from A to D is shown in figure 7.

Some results were also obtained for $\Delta = 3.462$, where there are two stable odd solutions (at J), four unstable odd solutions (at G, H) and two stable even solutions (at I). The first run was started from A with $q_0 = 0$, $C_0 = \frac{1}{2}\pi$ and converged to the unstable state at G; this is possible because the solution at G is only destabilized by the even part of a disturbance to ϕ and none is present. The solution at H cannot be selected, since it is destabilized by an odd component in ϕ. From a practical viewpoint it is now of interest to consider what the ultimate fate of the same solution would be if a small perturbation is introduced so that

$$q_0 = 0, \quad C_0 = \tfrac{1}{2}\pi - 0.1. \tag{8.7}$$

The solution initially approaches G, where it has the option of increasing q (with little change in C) to converge to the stable odd solution at J or of making a transition

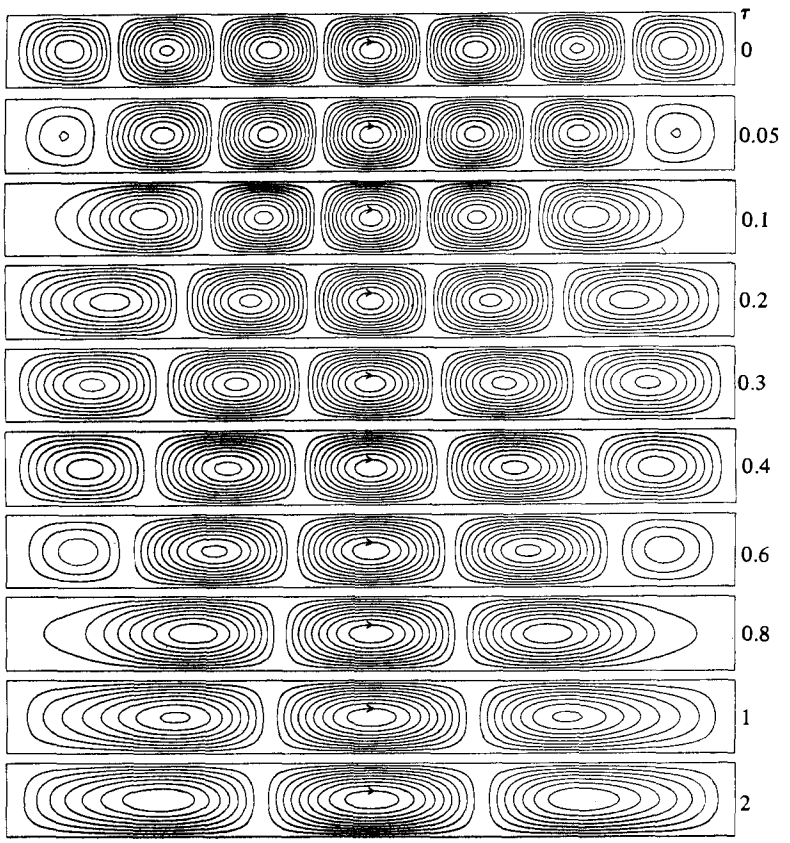

FIGURE 7. Streamline patterns at intervals of 0.25 for various values of τ for the transition of figure 6.

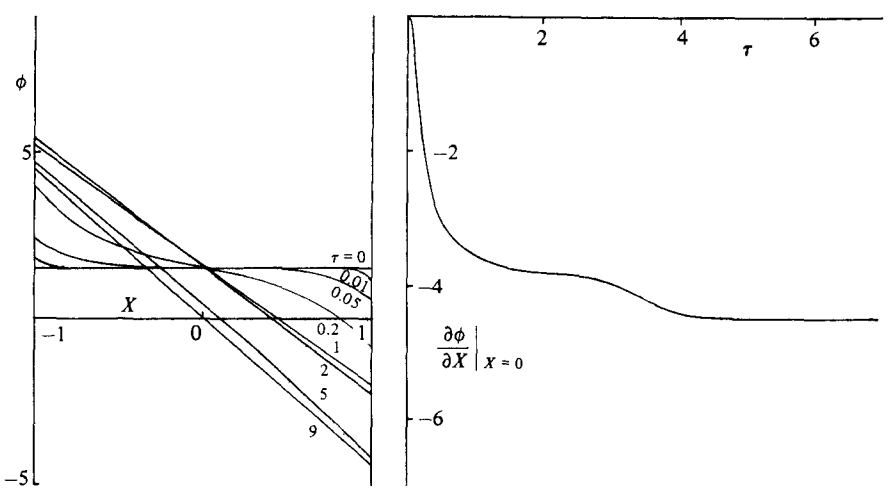

FIGURE 8. Properties of the solution $\phi(X,\tau)$ for the transition from the state (8.7) near A in figure 2 to the stable even state at I.

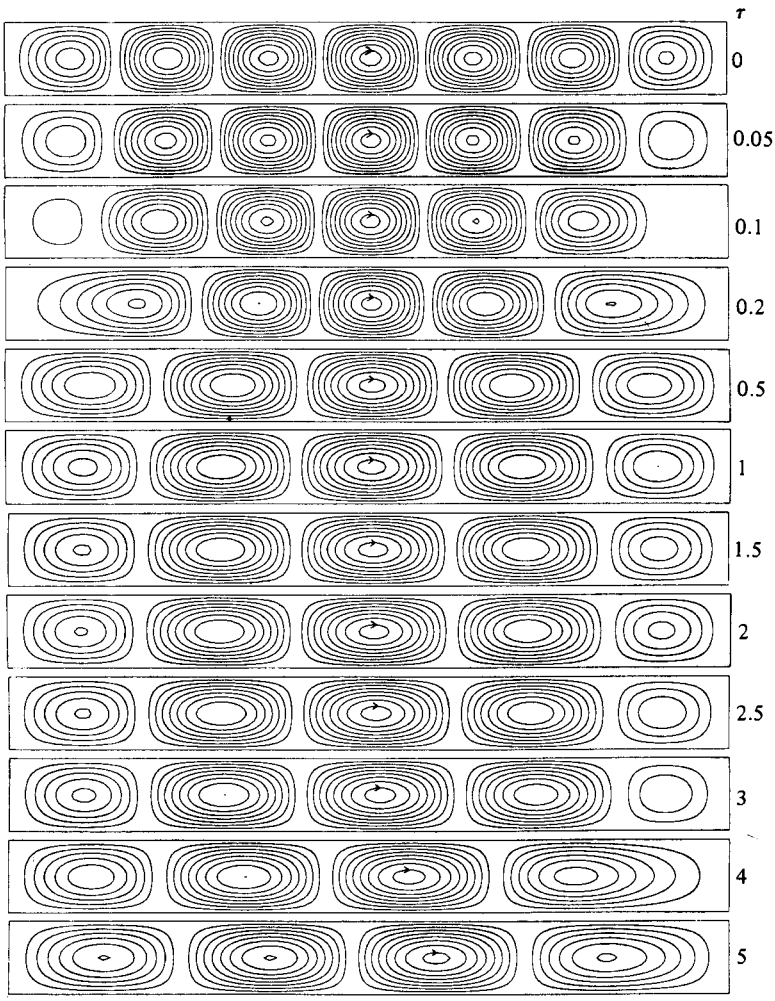

FIGURE 9. Streamline patterns at intervals of 0.25 for various values of τ for the transition of figure 8.

to the stable even solution at I. As shown in figures 8 and 9, the latter course was followed.

The results, including further tests in cases where a large number of steady-state solutions exist (e.g. $L = 10$, $P = \frac{1}{3}$, $\Delta = 15$, where there are sixteen class I solutions), seem to suggest that the following conclusions can be drawn. If the system starts from a stable configuration (necessarily either even or odd) then it will tend to preserve its even or odd nature after an increase in the Rayleigh number and will converge to the steady-state solution requiring the minimum change in the number of rolls, given that the solution must remain even or odd. (This means that a stable state may exist which would require a change in the number of rolls by one fewer than that which actually occurs.) The exception to this rule occurs if the solution so selected should happen to be unstable, which is a relatively rare occurrence for moderately high values of Δ. In these cases a small perturbation to the even part of ϕ is required to effect a transition from the even solution to the odd solution or vice versa. This transition involves a further change in the number of rolls by one. This last property

also suggests that if the Rayleigh number is raised by gradually incrementing its value by small amounts then in a situation such as that of figure 2 perturbations in the flow will result in these transitions as the maxima of the sinusoidal curves in figure 2 are encountered. The number of rolls will then decrease by one at each transition.

9. Discussion

This work describes the evolution of the roll pattern in a two-dimensional container of large aspect ratio $2L$ following a change in the Rayleigh number. Significant adjustments in the roll pattern take place if the Rayleigh number is changed by an amount order L^{-1}, although the prominent features of the evolution in the stress-free case are largely dependent on the value of the Prandtl number of the fluid which determines whether the number of rolls has to change. The mechanisms that affect the precise way in which changes in the roll pattern occur are described in detail in §§7 and 8 and are a subtle combination of the stability characteristics of the flow and of the tendency to preserve the symmetry of the system. In all cases the adjustment of the roll pattern is just the last of three stages of evolution. When $t = O(1)$ the basic temperature field adjusts to the new Rayleigh number. The amplitude of convection then adjusts accordingly when $t = O((R-R_0)^{-1}) = O(L)$, the lateral positioning of the rolls remaining unchanged during this time. However, the development of the boundary-layer region near each sidewall eventually penetrates into the core region when $t = O(L^2)$ and the roll pattern then changes. The adjustment is generally initiated at the sidewalls and spreads inwards to the centre of the container.

Although the main emphasis in the numerical study of §8 is on the evolution following an *increase* in Rayleigh number, the present analysis is equally applicable to the evolution produced by a decrease in Rayleigh number, and it is clear that in many cases the flow will exhibit hysteresis. The amplitude adjustment when $t = O(L)$ is still described by the results of §4, with the core behaviour given by (4.4) if $0 < \Delta_1 < \Delta_0$. If $\Delta_1 < 0$ the core solution (4.4) becomes

$$A_0 = \frac{\Delta_0^{\frac{1}{2}} |\Delta_1|^{\frac{1}{2}} e^{-|\Delta_1|\bar{\tau}+i\phi_0(X)}}{(\Delta_0+|\Delta_1|-\Delta_0 e^{-2|\Delta_1|\bar{\tau}})^{\frac{1}{2}}}, \tag{9.1}$$

and the entire motion decays to zero on this timescale, the final state now being a subcritical one.

The main drawbacks of the theory are the assumptions of two-dimensionality and stress-free horizontal boundaries, although it is not expected that the effect of rigid boundaries will necessitate any major changes. The main requirement is a knowledge of the parameters equivalent to α_0 and β in the rigid case, which will again depend upon the Prandtl number and will determine whether the evolution is of the simple type (figure 1) or the more interesting type (figure 2). This will, however, require a large amount of numerical work. Some support for the applicability of the present work is at least provided by numerical and experimental observations of two-dimensional rolls, although a proper extension of the present work to three-dimensional systems also presents a formidable task. It is expected that the present type of structure is of most relevance in relatively narrow channels where the rolls are approximately normal to the (narrow) channel walls at the onset of convection. Larger rectangular planforms (Brown & Stewartson 1977; Normand 1981; Greenside

et al. 1982) or cylindrical geometries (Brown & Stewartson 1978) are subject to the much wider class of three-dimensional instabilities that can lead to complicated roll patterns of the type elegantly described by Cross (1982).

Appendix A. Initial structure of the core solution in the final stage of evolution

In this appendix the solution of the system (7.1) is described for $\tau \ll 1$ and it is shown to be consistent with the terminal behaviour of the boundary-layer evolution as $\tilde{\tau} \to \infty$.

For $-1 < X < 1$ the solution evolves from the initial profile $\phi_0(X)$ in the form

$$\phi \sim \sum_{n=0}^{\infty} \phi_n(X)\tau^n, \tag{A 1}$$

where

$$\phi_n = \frac{1}{n!}\frac{\mathrm{d}^{2n}\phi_0}{\mathrm{d}X^{2n}}. \tag{A 2}$$

This solution does not satisfy the boundary conditions at $X = \pm 1$, and near $X = -1$ there is a region where $\eta = (X+1)/\tau^{\frac{1}{2}} = O(1)$ and

$$\phi \sim \phi_0(-1) + \sum_{n=1}^{\infty} g_n(\eta)\tau^{\frac{1}{2}n}. \tag{A 3}$$

Substitution into the governing equation shows that g_n satisfies the equation

$$g_n'' + \tfrac{1}{2}\eta g_n' - \tfrac{1}{2}n g_n = 0 \quad (n \geqslant 1), \tag{A 4}$$

while the boundary condition at $X = -1$ requires that

$$\sum_{n=1}^{\infty} g_n'(0)\tau^{\frac{1}{2}(n-1)} = -\tfrac{1}{2}\mathcal{A}(\alpha_0 + |\beta| \sin\{2\phi_0(-1) + \chi + \sum_{n=1}^{\infty} \tau^{\frac{1}{2}n} g_n(0)\}). \tag{A 5}$$

Equating coefficients of $\tau^{\frac{1}{2}(n-1)}$ on each side then gives

$$g_n'(0) = l_n \quad (n \geqslant 1), \tag{A 6}$$

where l_n can be determined in terms of the values of $g_i(0)$, $i = 1, \ldots, n-1$. The first few are

$$\left.\begin{aligned} l_1 &= -\tfrac{1}{2}\mathcal{A}(\alpha_0 + |\beta| \sin\{2\phi_0(-1) + \chi\}), \\ l_2 &= -\tfrac{1}{2}\mathcal{A}\,|\beta|\, g_1(0) \cos\{2\phi_0(-1) + \chi\}, \\ l_3 &= -\tfrac{1}{2}\mathcal{A}\,|\beta|\, (g_2(0) \cos\{2\phi_0(-1) + \chi\} - \tfrac{1}{2} g_1(0)^2 \sin\{2\phi_0(-1) + \chi\}). \end{aligned}\right\} \tag{A 7}$$

The boundary conditions for g_n are completed by the requirement of matching with the core solution (A 1), which implies

$$g_n \sim \frac{\eta^n}{n!}\frac{\mathrm{d}^n\phi_0}{\mathrm{d}X^n}(-1) \quad \text{as} \quad \eta \to \infty \quad (n \geqslant 1). \tag{A 8}$$

The solution of (A 4), (A 6) and (A 8) can be given in terms of parabolic-cylinder functions U and V (see Abramowitz & Stegun 1964, p. 686) as

$$g_n = \mathrm{e}^{-\frac{1}{8}\eta^2}\left\{\bar{a}_n\, U\left(n+\tfrac{1}{2}, \frac{\eta}{\sqrt{2}}\right) + \bar{b}_n\, V\left(n+\tfrac{1}{2}, \frac{\eta}{\sqrt{2}}\right)\right\} \quad (n \geqslant 1), \tag{A 9}$$

where

$$\bar{b}_n = \frac{\pi^{\frac{1}{2}} 2^{\frac{1}{2}(n-1)}}{n!}\frac{\mathrm{d}^n\phi_0}{\mathrm{d}X^n}(-1) \quad (n \geqslant 1), \tag{A 10}$$

and

$$\left.\begin{aligned} \bar{a}_{2m} &= -2^{m+\frac{1}{2}}\pi^{-\frac{1}{2}}(m-\tfrac{1}{2})!\,l_{2m} \\ \bar{a}_{2m+1} &= -\frac{2^{m+1}m!}{\pi^{\frac{1}{2}}}\left\{l_{2m+1}+\frac{(-1)^m 2^{2m+1}\pi^{\frac{1}{2}}}{(2m+1)!\,(-m-\frac{3}{2})!}\frac{\mathrm{d}^{2m+1}\phi_0}{\mathrm{d}X^{2m+1}}(-1)\right\} \quad (m \geqslant 0). \end{aligned}\right\} \tag{A 11}$$

The leading-order solution is

$$g_1 = \mathrm{e}^{-\frac{1}{8}\eta^2}\left\{\pi^{\frac{1}{2}}\phi_{0X}(-1)\,V\left(\tfrac{3}{2},\frac{\eta}{\sqrt{2}}\right)+2\pi^{-\frac{1}{2}}[\phi_{0X}(-1)-l_1]\,U\left(\tfrac{3}{2},\frac{\eta}{\sqrt{2}}\right)\right\}, \tag{A 12}$$

and by expressing g_1' in terms of the error function it can be verified that this is equivalent to the asymptotic solution (5.23) in the boundary layer.

If the initial profile is one of the steady-state solutions of the system, $\phi_{0XX} = 0$ and the central region $-1 < X < 1$ remains undisturbed until it is influenced by the spread and eventual interaction of the two boundary layers when $\tau = O(1)$, to produce the final steady-state configuration. Physically this corresponds to the initial development of the new roll pattern from the sidewalls of the container, a feature that can be observed in the numerical results of §8.

Appendix B. Analytic solution of the final evolutionary system for small Δ

A complete analytic solution of the system (7.1) is possible for Rayleigh numbers close to critical, $\Delta \ll 1$. In the initial stage when $\tau = O(1)$,

$$\phi = \phi^{\mathrm{A}}(X,\tau)+\Delta\phi^{\mathrm{B}}(X,\tau)+\ldots, \tag{B 1}$$

where the equations and initial conditions are

$$\phi^{\mathrm{A,B}}_{\tau} = \phi^{\mathrm{A,B}}_{XX}, \quad \phi^{\mathrm{A,B}}(X,0) = \phi^{\mathrm{A,B}}(X). \tag{B 2}$$

If the initial conditions arise from the flow configuration at a Rayleigh number also close to critical we would have $\phi^{\mathrm{A}}(X) = \frac{1}{2}n\pi, \phi^{\mathrm{B}}(X) = q_0 X/\Delta$, but this assumption is not a prerequisite of the analysis; the solution can be construed, for example, as that following a decrease in the Rayleigh number from a finite value $\Delta_0 > 0$. The boundary conditions for ϕ^{A} and ϕ^{B} are

$$\phi^{\mathrm{A}}_X(\pm 1,\tau) = 0, \quad \phi^{\mathrm{B}}_X(\pm 1,\tau) = -\tfrac{1}{2}(\alpha_0 \mp |\beta| \sin\{2\phi^{\mathrm{A}}(\pm 1,\tau)\mp\chi\}). \tag{B 3}$$

The solution for ϕ^{A} can be expressed as

$$\left.\begin{aligned} \phi^{\mathrm{A}}(X,\tau) &= \tfrac{1}{2}a_0+\sum_{m=1}^{\infty} a_m\,\mathrm{e}^{-\frac{1}{4}m^2\pi^2\tau}\cos\tfrac{1}{2}m\pi(X+1), \\ a_m &= \int_{-1}^{1}\phi^{\mathrm{A}}(X)\cos\tfrac{1}{2}m\pi(X+1)\,\mathrm{d}X, \end{aligned}\right\} \tag{B 4}$$

so that in general there will be an adjustment in the roll pattern, with

$$\phi^{\mathrm{A}}(X,\tau)\to\tfrac{1}{2}a_0 \quad \text{as} \quad \tau\to\infty. \tag{B 5}$$

It then follows that

$$\phi^{\mathrm{B}}(X,\tau) \sim d_0\tau+d_1+d_2 X+d_3 X^2 \tag{B 6}$$

as $\tau\to\infty$, where, from (B 2),

$$2d_3 = d_0 \tag{B 7}$$

and, from (B 3),

$$\left.\begin{aligned} d_2-2d_3 &= -\tfrac{1}{2}(\alpha_0+|\beta|\sin\{a_0+\chi\}),\\ d_2+2d_3 &= -\tfrac{1}{2}(\alpha_0-|\beta|\sin\{a_0-\chi\}),\end{aligned}\right\} \tag{B 8}$$

so that the constants d_0, d_2 and d_3 can be determined as

$$d_0 = \tfrac{1}{2}|\beta|\cos\chi\sin a_0, \quad d_2 = -\tfrac{1}{2}\alpha_0-\tfrac{1}{2}|\beta|\sin\chi\cos a_0, \quad d_3 = \tfrac{1}{4}|\beta|\cos\chi\sin a_0. \tag{B 9}$$

Thus as $\tau\to\infty$

$$\phi \sim \tfrac{1}{2}a_0+\Delta(d_0\tau+d_1+d_2X+d_3X^2), \tag{B 10}$$

indicating a second stage of evolution when $\tau\sim\Delta^{-1}$.

A longer timescale τ_1 is defined by

$$\tau_1 = \Delta\tau, \tag{B 11}$$

and a solution for ϕ constructed in the form

$$\phi = D_0(\tau_1)+\Delta(D_1(\tau_1)+D_2(\tau_1)X+D_3(\tau_1)X^2)+O(\Delta^2). \tag{B 12}$$

From terms of order Δ in (7.1)

$$D_{0_{\tau_1}} = 2D_3 \tag{B 13}$$

and

$$\left.\begin{aligned} D_2-2D_3 &= -\tfrac{1}{2}(\alpha_0+|\beta|\sin\{2D_0+\chi\}),\\ D_2+2D_3 &= -\tfrac{1}{2}(\alpha_0-|\beta|\sin\{2D_0-\chi\}).\end{aligned}\right\} \tag{B 14}$$

After elimination of D_2 and D_3 this yields a single equation for D_0:

$$D_{0_{\tau_1}} = \tfrac{1}{2}\beta_r\sin 2D_0, \quad D_0(0) = \tfrac{1}{2}a_0. \tag{B 15}$$

The required solution is the branch of

$$D_0 = \mathrm{Tan}^{-1}(e^{\beta_r\tau_1}\tan\tfrac{1}{2}a_0) \tag{B 16}$$

that passes through $\frac{1}{2}a_0$ at $\tau_1 = 0$, and then

$$D_2 = -\tfrac{1}{2}\alpha_0-\tfrac{1}{2}\beta_i\left\{\frac{1-e^{2\beta_r\tau_1}\tan^2\frac{1}{2}a_0}{1+e^{2\beta_r\tau_1}\tan^2\frac{1}{2}a_0}\right\}, \quad D_3 = \frac{\beta_r e^{\beta_r\tau_1}\tan\frac{1}{2}a_0}{2\{1+e^{2\beta_r\tau_1}\tan^2\frac{1}{2}a_0\}}. \tag{B 17}$$

If the initial configuration is a steady-state solution with $\phi^A = \frac{1}{2}n\pi$, then $a_0 = n\pi$, and d_0 and d_3 are zero in (B 9). Convergence to the final state is completed when $\tau = O(1)$, with the even part of ϕ always given by $\frac{1}{2}n\pi$ and thus no change in the even or odd nature of the roll pattern. In the final state $q = \Delta d_2 = -\frac{1}{2}\Delta(\alpha_0+(-1)^n\beta_i)$ from (B 9), and this final state may be stable or unstable depending on the value of n.

However, if ϕ^A contains an even perturbation to $\frac{1}{2}n\pi$, $a_0 \neq n\pi$ and the solutions (B 16) and (B 17) are generated on the longer timescale $O(\Delta^{-1})$. If $\beta_r > 0$ an odd state ($C_0\to\frac{1}{2}n\pi$, n odd) is achieved as $\tau_1\to\infty$, while if $\beta_r < 0$ an even state ($C_0\to\frac{1}{2}n\pi$, n even) is achieved, the corresponding values of q being $\frac{1}{2}\Delta(\beta_i-\alpha_0)$ and $-\frac{1}{2}\Delta(\beta_i+\alpha_0)$ respectively. This is consistent with the stability criterion (7.5), which for $\Delta \ll 1$ reduces to $(-1)^n\beta_r < 0$.

The solution (B 16) is useful in providing an analytical description of the transition, already mentioned in §7, that can occur between an even and odd solution and as exhibited, for example, in the results of figures 4 and 8. In figure 4 the two timescales predicted by the above analysis are easily discernible. In figure 8 the situation is more

realistic, since the initial configuration, unlike that of figure 4, is a stable one, but now the timescales are less distinct in view of the larger value of Δ.

Finally, it should be noted that the above analysis contains the essential ingredients of the final evolution for Rayleigh numbers in the range $R-R_0 = O(L^{-2})$ when the long timescale (B 11) on which the even or odd nature of the roll pattern is established becomes $t = O(L^3)$. There is now also a shorter timescale $t = O(L^2)$ when the shape of the core amplitude profile (now a function of X) is adjusted. Transitions restricted to this regime are clearly of minor interest, however, in view of the fact that there are just two stable solutions and these contain a fixed number of rolls.

REFERENCES

Abramowitz, M. & Stegun, I. A. 1964 *Handbook of Mathematical Functions.* Dover.

Brown, S. N. & Stewartson, K. 1977 *Stud. Appl. Maths* **57**, 187.

Brown, S. N. & Stewartson, K. 1978 *Proc. R. Soc. Lond.* A **360**, 455.

Coles, D. 1965 *J. Fluid Mech.* **21**, 385.

Cross, M. C. 1982 *Phys. Rev.* A **25**, 1065.

Cross, M. C., Daniels, P. G., Hohenberg, P. C. & Siggia, E. D. 1980 *Phys. Rev. Lett.* **45**, 898.

Cross, M. C., Daniels, P. G., Hohenberg, P. C. & Siggia, E. D. 1983 *J. Fluid Mech.* **127**, 155.

Daniels, P. G. 1977 *Proc. R. Soc. Lond.* A **358**, 173.

Daniels, P. G. 1978 *Mathematika* **25**, 216.

Daniels, P. G. 1981 *Proc. R. Soc. Lond.* A **378**, 539.

Greenside, H. S., Coughran, W. M. & Schryer, N. L. 1982 *Phys. Rev. Lett.* **49**, 726.

Koschmieder, E. L. & Pallas, S. G. 1974 *Intl J. Heat Mass Transfer* **17**, 991.

Newell, A. C. & Whitehead, J. A. 1969 *J. Fluid Mech.* **38**, 279.

Normand, C. 1981 *J. Appl. Math. Phys.* **32**, 81.

Segel, L. A. 1969 *J. Fluid Mech.* **38**, 203.

Siggia, E. D. & Zippelius, A. 1981 *Phys. Rev.* A **24**, 1036.